

Swelling and Residual Bond Orientations of Polymer Model Gels: The Entanglement-Free Limit

Michael Lang,* Reinhard Scholz, Lucas Löser, Carolin Bunk, Nora Fribiczler, Sebastian Seiffert, Frank Böhme, and Kay Saalwächter



Cite This: *Macromolecules* 2022, 55, 5997–6014



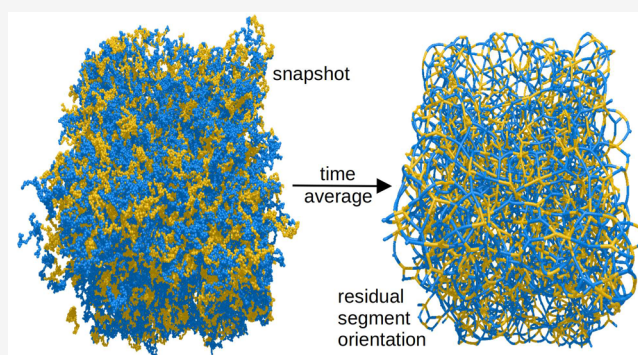
Read Online

ACCESS |

Metrics & More

Article Recommendations

ABSTRACT: We investigate the swelling of polymer model networks prepared at different polymer volume fractions and in solvents of different quality. We extend the existing theory to describe residual bond orientations (the vector and the tensor order parameters) for theta, good, and athermal solvents and put these relations in context with modulus at preparation conditions and the equilibrium degree of swelling. We find good agreement with the assumption of affine swelling for the weakly entangled networks of our study. The same scaling relations (up to numerical coefficients) are obtained for the vector order parameter, m , and the tensor order parameter, S , as a function of the preparation conditions, network structure, the equilibrium degree of swelling, Q , and the modulus at swelling equilibrium, G . We obtain $m \propto Q^{-2}$ and $G \propto m^{3/2}$ for swelling in theta solvents and $m \propto Q^{-1.08}$ with $G \propto m^{2.14}$ in the good-solvent regime, in both cases independent of preparation conditions. Modulus and residual bond orientation are related by $G \propto \phi_0 m$ and $G \propto \phi_0^{1.23} m$ as a function of the preparation polymer volume fraction ϕ_0 for theta solvents and good solvents, respectively. Computer simulations and experimental data for the good-solvent regime show good agreement with the predictions.



1. INTRODUCTION

Polymer gels consist of a network structure establishing the elasticity of the gel and a solvent that can be used to adjust the volume, and thus material properties like the modulus or the permeability of the gel. Adding solvents is often advantageous for synthesis and it allows optimization of the material properties in a particular application that can be as diverse as sustainable energy storage, water resource management, responsive materials, filters, or contact lenses,^{1,2} to provide just some examples.

Despite almost a century of academic research on rubber elasticity and the swelling of polymer networks, several key features of these materials are still not completely understood. For instance, widely accepted models for the swelling process of homogeneous networks are built upon the assumption of an affine deformation of the network strands.^{3–5} However, simulation studies have not confirmed an affine deformation process on the scale of individual network strands.^{6,7} From a theoretical point of view, it was proposed that a crossover in the swelling of network strands occurs from a subaffine swelling below the “affine length”⁸ to an affine swelling on large scales. It was also argued that subaffine swelling on short scales requires a des-interdispersion of network strands (a reduction of the overlap

number of the polymer strands). In fact, such a process was necessary to describe the equilibrium swelling of Olympic gels.⁹

The most direct way to analyze the microscopic processes during swelling is to monitor this process by computer simulations. Preceding simulation results on the affinity of swelling are difficult to interpret, since the analysis focused on instantaneous conformations^{6,7} instead of time-averaged conformations. Only the latter deform affinely within the classical models of rubber elasticity.¹⁰ The long-time mean-square displacements (MSD) of the monomers around these positions are expected to grow during swelling in nonentangled systems with the same scaling as the size of the elastic chains in a solution at the same polymer concentration.⁸ For entangled systems, it is expected that the virtual chains characterizing the topological constraints deform affinely and thus, release much of the entanglement constraints on the chains and network junctions upon swelling.¹¹ Therefore, it is quite interesting to analyze chain conformations and the dynamics of the cross-links in the swollen state. To the best of our knowledge, a detailed simulation study providing these details of the swelling process

Received: March 22, 2022

Revised: May 3, 2022

Published: July 15, 2022



<https://doi.org/10.1021/acs.macromol.2c00589>
Macromolecules 2022, 55, 5997–6014

for a broad range of different networks is not at hand. Even for the preparation state, such information is hard to find and does not cover a broad range of preparation conditions.¹² One remarkable result of that work was that the MSD of the cross-links connected by mildly entangled chains were more than 1 order of magnitude smaller than the mean-square end-to-end distances of the chains. These unexpectedly small cross-link displacements were confirmed in later works^{13–15} and discussed in some more detail in ref 16.

Experimental data provides mainly indirect evidence on the microscopic processes related to swelling, and it is sometimes hard to interpret. For instance, it was found that the entanglement contribution to the modulus should vanish at a nonzero polymer concentration,¹⁷ while it vanishes at zero concentrations using a different analysis.¹⁸ Moreover, the formation of network defects and cyclic structures is a function of the overlap of the chains.^{19,20} Therefore, corrections are necessary²¹ to discuss the dependence on the polymer volume fraction at preparation, ϕ_0 , which were developed recently^{22,23} and are still under debate.²⁴

This complex situation can be simplified when using a heterocomplementary coupling of star polymers that suppresses the formation of cyclic structures made of an odd number of elastic strands. This procedure was developed in ref 25 and it strongly increases the stability of the networks in the vicinity of the overlap concentration²⁶ while minimizing the corrections to modulus arising from finite loops²⁷ or other network defects. Yet, this architecture offers another possibility: the residual bond orientation of the smallest elastically active cyclic structure in the network differs significantly from all other elastically active strands.²⁰ This provides an experimental access to quantify loop defects in networks. We correct the theoretical discussion of preceding work²⁸ and derive a full set of relations for different solvent quality and as a function of ϕ_0 . These relations allow to connect with the properties of the dry sample, the fully swollen state, or samples swollen to equilibrium in solvents of different quality. The key predictions of theory are the residual orientations of the chain segments in the networks, which reflect either a long time average of the orientation vector of chain segments (the vector order parameter m) or of the orientation tensor (the tensor order parameter S) in case of a nondirected orientation. These order parameters range from zero for nonoriented segments to an upper bound (unity for m and $3/5$ for S) that refers to static segments that cannot move. In the absence of entanglements, the residual orientation inside polymer networks is mainly a measure of the force acting on the chain segments with some corrections related to conformations.¹⁵ In entangled networks, the mobility of the chain segments plays a vital role and modifies the scaling of the residual orientations.¹⁵ Our predictions are tested with computer simulations covering mainly the nonentangled good-solvent limit. Additional experimental data were collected at preparation conditions and at swelling equilibrium for a set of networks made of two batches of star polymers that were coupled using the heterocomplementary amine-oxazinone reaction as described earlier^{29,30} for Sakai's heterocomplementary coupling scheme. These data are also compared with the model predictions.

This work is structured as follows. In Section 2, we briefly describe the simulation method, the samples, and the data analysis. Further details on data analysis can be found in the Appendix. In Section 3, we analyze to what extent swelling refers to an affine displacement of the cross-link positions. Section 4

deals with the elastic properties and the residual bond orientations in the preparation state. We develop the theory and compare with data from simulations and experiment. Section 5 discusses equilibrium swelling and residual bond orientations in the swollen state. Here, we present simulation and experimental data in comparison with scaling predictions for bond orientations and the degree of swelling. A detailed derivation of all scaling predictions of this section can be found in the Appendix along with scaling predictions of the bond orientation in deswollen networks. All results are put into a broader context in Section 6, with the key findings summarized at the end of this work.

2. SIMULATIONS, EXPERIMENTS, AND DATA ANALYSIS

2.1. Simulations. Simulations are performed with the bond fluctuation model (BFM)^{31,32} in the framework of LeMon-ADE^{33,34} on graphical processing units (GPU). The BFM is suitable for the coarse-grained simulations of a broad variety of systems like melts, solutions, hyper-branched molecules, brushes, and other problems of polymer physics.^{35–38} Since this method is very efficient, it was frequently used to model polymer networks and their swelling.^{7,39–41}

In the BFM, a monomer is modeled by cubes occupying 8 adjacent lattice sites of a simple cubic lattice. A coarse grained polymer is established by monomers connected through bonds which comply with a set of 108 bond vectors. Within one Monte Carlo-Step (MCS), it is attempted to move each monomer to one of the six nearest neighboring positions on the lattice under the constraints of the excluded volume of other monomers and the set of allowed bond vectors to the connected monomers. Polymers are either entangled or not, depending on the choice of the bond vectors^{32,42} for moves along the lattice directions. We have chosen the same bond vector set as in preceding work⁴³ in order to model entangled polymers. Empty lattice sites serve as an implicit a-thermal solvent. Boundary conditions were set to nonperiodic to allow subsequent swelling of the networks by placing the samples in a larger simulation container.

We created solutions of star polymers at concentrations varying by more than 1 order of magnitude from below the overlap volume fraction ϕ^* up to melt conditions. For our simulation model, these are reached^{30,32} at $\phi \gtrsim 0.4$ and a volume fraction of $\phi = 0.5$ was considered previously as “standard” to simulate “melts”.^{44–46}

After insertion of the star polymers, the samples were relaxed over 10^7 Monte Carlo Steps (MCS). For obtaining a rough idea of polymer relaxation times in units of MCS, we mention that chains with $N = 82$ segments relax faster than 10^6 MCS at the largest densities studied, see for example ref 47. The degrees of polymerization of the two batches of star polymers were chosen to be roughly comparable to the recent experiments³⁰ and to preceding works on tetra-PEG networks.^{20,25} We use a heterocomplementary coupling between the two batches of stars²⁵ at stoichiometric conditions to eliminate the formation of pending loops.^{20,26} When connected, the number of chain segments between two star centers, N , reaches values of $N = 23$, 43, and 82 (number of monomers between star centers is $N - 1$). All M stars carry four arms, $f = 4$, and all systems are reacted up to a conversion of exactly $p = 0.95$ using the same algorithm as described in ref 27. The advantage of this procedure is that corrections regarding conversion and kinetics cancel for analyzing the simulation data.⁴⁸ Enforcing constant p leads to somewhat different trends with respect to the experiments.

Table 1. Parameters of the Simulations and Key Results^a

<i>N</i>	ϕ_0	ϕ_1	<i>L</i>	<i>M</i>	w_{sol}	w_{act}	<i>I₄</i>	<i>I₂R₂</i>	$\frac{R_0^2}{R^2}$	$\frac{\delta R_0^2}{R^2}$	<i>m₀</i>	<i>m₀(I)</i>	<i>m₀(R₂)</i>	<i>Q</i>	$\frac{R^2}{R_0^2}$	$\frac{\langle R \rangle^2}{R^2}$	$\frac{\delta R^2}{R^2}$	<i>m</i>	<i>m(I)</i>	<i>m(R₂)</i>	
82	0.373	0.377	256	4800	0.13	93.13	73.0	10.4	134.5	113.0	11.1	0.0262	0.0282	0.0188	15.56	374.7	343.6	17.2	0.0812	0.0869	0.0628
82	0.311	0.317	256	4000	0.07	92.94	70.8	12.7	141.0	116.0	13.1	0.0252	0.0274	0.0176	17.32	374.1	338.8	20.4	0.0745	0.0803	0.0566
82	0.249	0.255	256	3200	0.06	92.86	71.8	12.2	148.4	118.7	15.9	0.0244	0.0265	0.0165	19.38	366.9	325.9	25.0	0.0666	0.0719	0.0482
82	0.187	0.194	256	2400	0.08	92.43	69.9	14.1	165.5	127.2	20.0	0.0242	0.0265	0.0157	21.82	361.8	313.8	30.2	0.0589	0.0641	0.0410
82	0.124	0.132	256	1600	0.06	92.67	66.9	16.5	188.1	141.9	27.0	0.0246	0.0272	0.0151	25.15	354.3	297.1	39.0	0.0504	0.0555	0.0335
82	0.093	0.097	512	12800	0.18	92.62	67.2	16.7	188.7	144.3	26.6	0.0245	0.0272	0.0155	24.96	347.1	294.1	34.5	0.0493	0.0545	0.0326
82	0.062	0.067	512	6400	0.16	92.63	59.8	23.6	223.2	158.9	43.3	0.0233	0.0266	0.0136	34.57	329.6	259.6	53.3	0.0378	0.0430	0.0227
82	0.047	0.051	512	4800	0.27	92.17	56.4	26.7	237.6	165.7	50.8	0.0231	0.0270	0.0131	37.95	319.1	242.0	62.3	0.0338	0.0393	0.0198
82	0.031	0.036	512	3200	0.45	91.98	49.5	31.7	257.3	174.0	64.8	0.0228	0.0274	0.0134	44.07	308.1	221.6	76.1	0.0290	0.0346	0.0173
82	0.023	0.029	512	2400	0.42	91.87	43.7	36.5	265.8	174.5	76.7	0.0221	0.0271	0.0137	47.04	299.2	205.6	86.9	0.0259	0.0318	0.0160
82	0.016	0.022	512	1600	0.81	90.20	33.8	40.6	275.0	175.4	95.6	0.0201	0.0265	0.0125	52.88	293.7	190.6	106.0	0.0221	0.0289	0.0139
43	0.389	0.394	256	9600	0.13	92.66	69.6	14.4	72.2	57.4	8.2	0.0398	0.0436	0.0287	13.00	174.5	155.4	12.0	0.1073	0.1165	0.0782
43	0.259	0.266	256	6400	0.17	92.71	68.0	15.7	79.5	60.2	11.3	0.0382	0.0421	0.0238	15.34	166.4	142.8	16.0	0.0891	0.0977	0.0600
43	0.195	0.202	256	4800	0.17	92.58	64.8	18.6	85.9	63.0	14.1	0.0373	0.0418	0.0228	17.20	161.5	134.6	19.6	0.0782	0.0870	0.0506
43	0.195	0.198	512	38400	0.16	92.67	67.1	16.7	86.8	64.7	13.8	0.0387	0.0429	0.0235	16.84	159.3	134.1	17.3	0.0788	0.0869	0.0510
43	0.130	0.134	512	25600	0.13	92.55	63.2	20.2	96.6	69.4	18.3	0.0383	0.0432	0.0229	20.40	155.4	125.8	22.5	0.0685	0.0768	0.0429
43	0.097	0.102	512	19200	0.22	92.44	60.5	22.6	105.9	73.0	22.1	0.0385	0.0440	0.0222	22.56	150.6	118.0	26.5	0.0616	0.0702	0.0364
43	0.065	0.070	512	12800	0.27	92.19	53.8	28.5	113.6	77.4	28.5	0.0383	0.0450	0.0224	25.72	144.4	107.3	33.4	0.0528	0.0620	0.0311
43	0.049	0.054	512	9600	0.22	91.98	50.2	31.0	119.5	79.9	33.4	0.0382	0.0457	0.0228	27.93	139.9	99.8	38.8	0.0476	0.0569	0.0285
43	0.032	0.039	512	6400	0.45	91.72	41.7	36.3	126.4	81.4	44.2	0.0366	0.0457	0.0228	32.17	136.1	91.2	48.1	0.0410	0.0509	0.0257
43	0.024	0.032	512	4800	0.26	90.95	33.4	41.3	128.9	79.0	55.8	0.0335	0.0437	0.0216	35.90	134.3	84.4	61.8	0.0358	0.0469	0.0228
43	0.016	0.025	512	3200	1.08	89.63	23.0	46.0	129.7	70.8	83.6	0.0272	0.0380	0.0188	43.57	131.7	72.9	84.9	0.0286	0.0400	0.0195
43	0.012	0.022	512	2400	1.70	86.75	16.5	44.3	130.7	65.7	108.8	0.0232	0.0348	0.0176	47.07	132.2	67.4	113.0	0.0239	0.0358	0.0180
23	0.412	0.417	256	19200	0.17	92.64	67.5	16.4	37.8	28.3	5.7	0.0608	0.0671	0.0394	10.33	77.6	66.8	7.5	0.1414	0.1549	0.0989
23	0.343	0.350	256	16000	0.13	92.73	65.7	17.8	39.4	29.1	6.5	0.0603	0.0669	0.0377	10.98	76.1	64.5	8.4	0.1315	0.1450	0.0880
23	0.275	0.282	256	12800	0.18	92.65	64.2	19.6	41.7	30.0	7.5	0.0600	0.0671	0.0367	11.91	74.0	61.3	9.7	0.1203	0.1337	0.0778
23	0.206	0.214	256	9600	0.18	92.59	62.0	21.6	44.7	31.5	9.0	0.0603	0.0680	0.0363	13.08	71.4	57.4	11.2	0.1080	0.1211	0.0687
23	0.137	0.146	256	6400	0.22	92.21	57.3	25.5	49.4	33.8	11.6	0.0611	0.0705	0.0363	14.75	68.4	52.4	14.4	0.0924	0.1061	0.0568
23	0.137	0.142	512	51200	0.17	92.35	58.4	24.5	49.8	34.5	11.7	0.0618	0.0709	0.0368	15.27	68.8	53.4	13.4	0.0947	0.1082	0.0576
23	0.103	0.108	512	38400	0.21	92.31	54.2	28.0	53.0	36.0	13.8	0.0623	0.0727	0.0375	16.66	66.7	49.8	15.5	0.0855	0.0996	0.0520
23	0.069	0.074	512	25600	0.27	92.02	46.0	34.4	57.0	37.7	17.8	0.0618	0.0746	0.0385	18.99	64.3	45.3	20.1	0.0740	0.0891	0.0465
23	0.051	0.059	512	19200	0.24	91.89	39.3	38.5	59.1	37.9	21.9	0.0598	0.0743	0.0383	20.92	63.0	42.1	23.9	0.0662	0.0823	0.0425
23	0.034	0.044	512	12800	0.59	90.71	28.2	44.4	60.7	36.2	33.0	0.0530	0.0704	0.0362	24.61	61.9	37.6	36.1	0.0549	0.0728	0.0375
23	0.026	0.037	512	9600	0.98	89.58	21.4	45.1	61.3	33.9	44.0	0.0467	0.0659	0.0334	27.82	61.8	34.4	47.3	0.0476	0.0671	0.0340
23	0.017	0.028	512	6400	2.82	85.42	12.1	43.2	61.2	27.7	81.0	0.0333	0.0527	0.0267	35.98	61.5	27.8	94.9	0.0333	0.0526	0.0268
23	0.013	0.023	512	4800	4.16	80.50	8.7	38.4	61.3	22.7	117.6	0.0253	0.0434	0.0220	47.59	61.8	23.0	126.1	0.0251	0.0434	0.0215
23	0.009	0.014	512	3200	16.71	22.84	4.9	27.9	61.0	12.5	241.6	0.0099	0.0230	0.0099	77.97	61.1	13.0	262.8	0.0104	0.0197	0.0107

^a*N* is the number of segments between network junctions, ϕ_0 and ϕ_1 are the nominal and the effective polymer volume fraction at preparation, *L* is the box size at preparation, and *M* the total number of star polymers. w_{sol} and w_{act} are the weight fractions of sol and of the elastically active material (in % of polymer mass), *I₄* and *I₂R₂* are the weight fractions of stars with four "ideal" connections and of stars involved in double links³⁰, respectively, both in % of network mass. *Q* is the equilibrium degree of swelling, m_0 , $m_0(I)$ and $m_0(R_2)$ are the vector order parameter for the full sample, for the ideal connections and the double links in the preparation state, respectively. The square size of ideal connections at preparation is R_0^2 , the time-averaged square size of these strands is $\langle R_0 \rangle^2$, and the time-averaged MSD of active network junctions is δR_0^2 . Without index "0", the last six quantities are measured at swelling equilibrium.

There, reactions are usually carried out over similar time spans, tending to lower conversions at lower concentrations. The parameters and key results of all simulations are summarized in Table 1.

Swelling simulations on a lattice are almost impossible when using period boundary conditions, since one would have to introduce additional lattice layers inside the network to enlarge the volume. The addition of extra lattice layers leads to bonds outside of the fixed bond vector set of the simulation model causing the chains to break. In order to avoid such problems, for each line of Table 1, a network was prepared in nonperiodic boundaries. After cross-linking, these networks were relaxed over 2.5×10^9 MCS and a snapshot of the conformations was taken every 10^6 MCS for all samples in a box with $L = 256$. For the samples in boxes $L = 512$, we collected data over 10^8 MCS in intervals of 10^5 MCS. In a subsequent step of the simulations, all networks were placed into a larger simulation container and swollen to equilibrium within the 10^8 MCS of this run. In equilibrium, we repeated the analysis with the same time window and frequency as in the preparation state.

2.2. Data Analysis. Regarding notation, we distinguish between preparation state, reference state (a polymer solution at the same polymer volume fraction ϕ), dry state ($\phi = 1$), and equilibrium swelling. Variables or observables in these states are distinguished by an index “0”, “ref”, and “dry”, respectively, while the equilibrium state carries no index. Thus, ϕ_0 is the polymer volume fraction at preparation, R_{ref} is the reference chain size of a polymer in a solution with same volume fraction as the equilibrium ϕ , G_{dry} is the modulus in the dry state, whereas m_0 is the vector order parameter at preparation conditions. Alternatively, the vector order parameter is called the “residual bond orientation” or simply “order parameter” in literature, thus also in this work. The key variables to characterize the networks are the average number of segments between two network junctions, N , the junction functionality, f , and the effective polymer volume fraction at preparation, ϕ_1 (see below for distinction between ϕ_0 and ϕ_1). Further examples to explain the notation are given in the caption of Table 1.

The weight fraction of sol, w_{sol} , is computed as the weight fraction of all clusters except for the largest one. The weight fraction of the elastically active material, w_{act} , is determined using the definition of Scanlan and Case.^{49,50} For the full sample, we determine the fractions of stars with exactly 4 connections to 4 different stars, I_4 , and the stars with exactly one double link to the same partner and two connections to two other stars, I_2R_2 , see ref 26 for more details. These two species dominate the different types of connectivity among the star polymers for a broad range of concentrations,²⁶ see Table 1. Both can be quantified with a special proton NMR technique, that is, proton multiple-quantum (MQ) NMR.²⁰

In our analysis of chain conformations, we focus on active chains I that are not part of a double or a multiple link (“ideal connections”). Sample averages over all chains show systematic shifts due to the increasing fraction of R_2 with increasing dilution. The ensemble average chain size is computed as R^2 , time-averaged square size of individual chains (averaged over the sample in a second step) are denoted as $\langle R \rangle^2$, and the time-averaged MSD of the active cross-links around their time-averaged position is given as δR^2 . All sizes are normalized by the particular mean-square size of a bond in the simulation container, b_0 or b , to cancel the concentration dependence of the bond length.

The average residual bond orientation is extrapolated toward infinite time as described in ref 51, see also the Appendix. Similar to preceding work,^{20,27} we provide data for the vector order parameter m averaged over all segments, for the “ideal” connections (strand is the only connection between a pair of stars) inside the active material, $m(I)$, and for all “double links”, $m(R_2)$, (two connections between the same pair of stars) inside the network. Table 1 contains all data for preparation state and equilibrium swelling, respectively.

The hard boundaries of the simulation container lead to a drop of the concentration of the polymer solution in its vicinity. The polymer volume fraction is near zero directly at the boundary and increases within a correlation length ξ to an effective average polymer volume fraction $\phi_1 > \phi_0$. Therefore, we have used the same algorithm for determining Q (described in the Appendix) also for the samples in the preparation container to compute the effective polymer volume fraction during the cross-linking process, ϕ_1 . The Appendix shows one example for this analysis.

2.3. Experiments. In parallel to the simulations, we conducted several experiments described in detail in a second paper.³⁰ In brief, two batches of star polymers (oxazinone-terminated tetra-arm star poly(ϵ -caprolactone) and amino-terminated tetra-arm poly(ethylene glycol)) were synthesized and reacted in a heterocomplementary fashion at different concentrations in different cosolvents (tetrahydrofuran, toluene, and chloroform) using the coupling mechanism described in ref 29. As shown in ref 30, these networks develop near model character similar to the tetra-PEG approach proposed originally by Sakai²⁵ and an equilibrium swelling behavior that is equivalent to homopolymers, if a good cosolvent for both polymers is used.

In the present work, we combine data from ref 30 and additional measurements to check the key results of our scaling discussion. Rheological measurements were performed on an Anton Paar modular compact rheometer of type MCR 302 (Anton Paar, Graz, Austria) equipped with a plate–plate geometry of type PP25 with a plate diameter of 25 mm. A Peltier plate was used to control the temperature and a solvent trap was used to prevent evaporation of the solvent. Gels were prepared from homogenized equimolar mixtures of stock solutions of both functionalized star polymers in a mold fitting exactly the dimension of the probe geometry. The mixture was allowed to react overnight at room temperature. Frequency sweeps were carried out at a shear strain of $\gamma = 0.01$ with frequencies in the range of $\omega = 0.5–100$ rad s^{-1} . The equilibrium degree of swelling of the gels used for rheology and of additional samples was measured gravimetrically and converted into a volume swelling degree. Residual bond orientations were derived from proton MQ NMR experiments using the Baum-Pines sequence,⁵² and performed on a Bruker MiniSpec mq20. Samples were measured in the preparation state and at swelling equilibrium with swelling directly from the preparation state. The data was evaluated using the 3 component-model published by Lange et al.²⁰ combined with a grid-search-based optimization method for the actual process of fitting the data, whose application on MQ data is described in ref 30. Results of this approach are estimates for the component fractions of ideal connections and I_2R_2 , and the residual dipolar coupling among the protons.

3. IS SWELLING AN AFFINE PROCESS?

One important feature of the affine^{53,54} and the phantom model^{55,56} of rubber elasticity is that the time-averaged positions of all network junctions deform affinely with the sample geometry. For isotropic swelling, the macroscopic deformation factor λ is related to the volume changes upon swelling

$$\lambda = \left(\frac{V}{V_0}\right)^{1/3} = \left(\frac{\phi_0}{\phi}\right)^{1/3} \quad (1)$$

between preparation at ϕ_0 and measurement at an arbitrary volume fraction ϕ . Here, V is the sample volume at swelling equilibrium and V_0 the sample volume at preparation conditions. The volume of the dry sample, V_{dry} is used to define the equilibrium degree of swelling

$$Q = \frac{V}{V_{\text{dry}}} \quad (2)$$

The local deformation of individual network chains is affine within the affine or phantom model, thus,

$$R = \lambda R_0 \quad (3)$$

In the following, N_e is the degree of polymerization of an entangled strand. Many models on entangled networks assume that the virtual chains describing topological constraints deform affinely with the sample deformation (for instance, the constrained junction model,^{57,58} the nonaffine tube models,^{11,59–61} or the slip-tube model⁶²). In consequence, the effective tube diameter, a , deforms nonaffinely¹¹

$$a \approx bN_e^{1/2}\lambda^{1/2} \quad (4)$$

leading to the prediction of a rather weak concentration dependence of the tube diameter in networks upon swelling¹¹

$$a \propto (\phi/\phi_0)^{-1/6} \quad (5)$$

We drop coefficients of order unity for scaling relations, which is expressed by using “ \approx ” instead of “=” in the corresponding equations. Entangled solutions develop a much stronger dependence of the tube diameter on the polymer volume fraction, since the chains in the solution can fully adjust conformations to the interactions with the solvent, while the entanglement constraints in a network are fixed at preparation conditions.⁶³

We analyze the affinity of the swelling process for the innermost 50% of all chains by focusing on the deformation of the “ideal connections” between active network junctions. This restriction allows for a simpler analysis as compared to using all active chains: in the latter case, the different number fraction of I_2R_2 as a function of the overlap of the star polymers leads to an additional drift of the average chain size as a function of ϕ_0 . Affinity of the swelling process is checked by dividing the “microscopic” change in volume per chain, $\langle R \rangle^3/\langle R_0 \rangle^3$, (based upon the time-averaged chain sizes) with the macroscopic volume change $Q\phi_0$, see Figure 1. We performed this analysis considering either ϕ_0 or ϕ_1 as polymer volume fraction at preparation.

Subaffine, $\phi_0 Q \langle R \rangle^3/\langle R_0 \rangle^3 < 1$, or affine deformations, $\phi_0 Q \langle R \rangle^3/\langle R_0 \rangle^3 = 1$ on the microscopic scale are expected from theoretical arguments for entangled and nonentangled samples, respectively, while superaffine swelling is a nonphysical process (chains would stretch locally more than necessary to swell the sample to swelling degree Q). Using ϕ_0 for the polymer volume

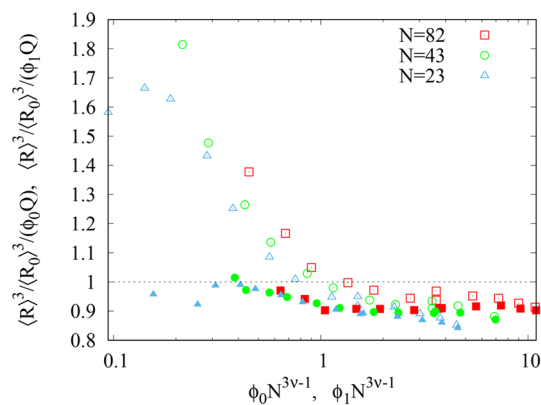


Figure 1. Test of affine microscopic deformations using time-averaged chain conformations in the preparation state, $\langle R_0 \rangle$ and at swelling equilibrium, $\langle R \rangle$. Open symbols show analysis based upon ϕ_0 , which is the nominal polymer volume fraction in the total simulation box. Full symbols show analysis based upon ϕ_1 , which is the polymer volume fraction in the inner part of the container as determined by the algorithm that analyzes the polymer volume fraction of swollen samples, see Appendix A for more details. The dashed line indicates affine deformations. Data below this line refers to subaffine deformation on the scale of individual network strands, data above this line refers to a nonphysical superaffine behavior.

fraction produces such nonphysical results. Plotting the data with ϕ_1 provides a transition from an affine swelling near the overlap polymer volume fraction where entanglements are least important to a weakly subaffine swelling process for large overlap numbers where all data remains near $\phi_0 Q \langle R \rangle^3/\langle R_0 \rangle^3 = 1$ or below. According to Figure 1, roughly 90% of the volume change can be explained by an affine deformation of the time-averaged network strands. The change in the time-averaged chain size agrees with the affine prediction within 5% for all samples of our study. Therefore, in the remainder of this work, we assume that swelling of weakly entangled networks (as in our study) is an affine process to a very good approximation. Moreover, we keep on using ϕ_0 to denote preparation conditions in all equations to stay consistent with literature notation. However, for all plots we use ϕ_1 instead of ϕ_0 in order to avoid nonphysical results. The error of the simulation data is typically comparable to the symbol size or smaller with one exception. This is visible in a rather low scatter of the data sets all plots where collapse of the data on a universal curve is observed. All figures with simulation data contain two samples per N with almost identical ϕ_1 that differ by a factor of 8 in volume at preparation conditions. The typical situation is that the two data points corresponding to this pair of systems are overlapping indicating only minor finite size corrections.

Before we proceed, we first check to which extent the networks of our study qualify as “ideal” reference systems. To put all data on a universal scale regarding connectivity, we introduce the overlap polymer volume fraction ϕ^* . For networks connected by junctions with a low functionality f , in the spirit of De Gennes work,⁶⁴ ϕ^* can be estimated by the overlap condition of the network strands

$$\phi^* \approx \left(\frac{v_K}{v}\right)^{6\nu-3} N^{1-3\nu} \quad (6)$$

Here, v is the excluded volume parameter characterizing the quality of the solvent, v_K is the volume of a Kuhn segment, and ν is the Flory exponent with⁶⁵ $\nu \approx 0.5876$. For our simulation

model, there is³⁰ $v/v_K \approx 0.39$ and $(v_K/v)^{6\nu-3} \approx 1.64$. Thus, the x -axis in Figure 2 corresponds roughly to the overlap number of

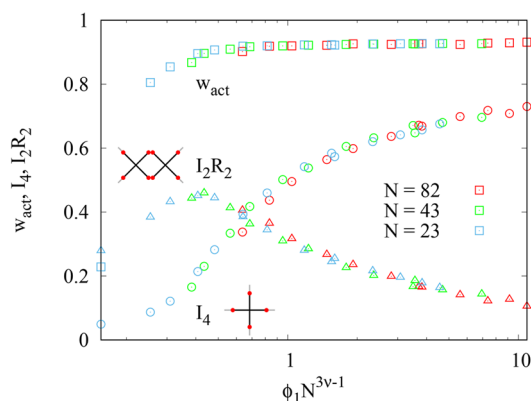


Figure 2. Squares show the weight fraction of the elastically active material, w_{act} , the circles display the weight fraction of star polymers with 4 connections to 4 different stars, I_4 , and the triangles are the weight fraction of stars that participate in a smallest loop, I_2R_2 . The corresponding connectivities are also sketched in the Figure, where the red dots are connections to other molecules and the gray lines indicate the continuation of the structure in the network.

the elastic strands at preparation conditions, ϕ_1/ϕ^* . The collapse of the data demonstrates that networks with the same overlap at preparation conditions develop an equivalent structure. w_{act} is nearly constant for $\phi N^{3\nu-1} > 1$. We expect a similar trend for experimental data if the conversion is very high, $p \approx 1$, and nearly constant as in our case. Since w_{act} is approximately constant for $\phi N^{3\nu-1} > 1$, the cycle rank per chain as a first order estimate of the elastic contribution per network chain is also nearly constant. The weight fraction of the stars in I_2R_2 connectivity is becoming significant around and below the overlap threshold, see Figure 2 also regarding a sketch of the I_2R_2 and the I_4 connectivity. Recall that small loops like R_2 reduce the modulus and increase the MSD of the cross-links.²³ A measurable drop of modulus and an increase of junction fluctuations around the overlap volume fraction is expected based upon these predictions for decreasing ϕ . Data at large overlap numbers are less affected by these corrections. Notably, I_4 and I_2R_2 establish more than 80% of all stars in the systems with $\phi_1 N^{3\nu-1} > 1$. This qualifies these networks for a quantitative analysis of these structures via NMR. Altogether, the networks are nearly ideal, in particular at large overlap of the stars, and we expect only small corrections for the phantom contribution to modulus and the junction fluctuations becoming more significant when approaching the overlap threshold.

The second fundamental aspect that we address is the way how the tube confinement changes upon swelling. For this analysis, we focus on the MSD of the network junctions. These are confined by entanglements and the constraints arising from the phantom modulus. For the entanglement constraints at preparation condition we assume^{66,67}

$$N_c(\phi) \approx N_c(\phi = 1)\phi^{-4/3} \quad (7)$$

For simplification, here, we have written down only the scaling in theta solvents, since the exponent for good solvents is almost identical numerically.⁶³ For an f -functional junction within an ideal phantom model network (no finite loops), network constraints are modeled by f virtual strands containing $K = (f - 1)N/(f - 2)$ segments each.^{23,63} We assume that the

connectivity of the system does not change much with dilution as we have enforced $p = 0.95$ for our simulations, and w_{act} is nearly constant for the systems of interest with $\phi_1 N^{3\nu-1} > 1$. Thus, to first order, K is constant. Cross-link MSDs increase with dilution predominantly through a swelling of the network chains, as described by the change of the reference size of the same chain in a polymer solution at ϕ_0 .⁶³

$$R_{\text{ref}}^2 \approx b^2 N \left(\frac{\phi^{**}}{\phi_0} \right)^{(2\nu-1)/(3\nu-1)} \propto \phi_0^{-0.23} \quad (8)$$

where

$$\phi^{**} \approx \frac{v}{v_K} \quad (9)$$

is the crossover concentration between the concentrated regime, $\phi_0 > \phi^{**}$, and the semidilute good-solvent regime, $\phi^{**} > \phi_0 > \phi^*$. For our simulation model, we have^{30,32} $\phi^{**} \approx 0.39$, thus all of our networks were prepared in the good-solvent regime. The cross-link confinement, $b_0^2/\delta R_0^2$, is the inverse of the cross-link MSDs. For this confinement, we adapt preceding work¹⁶ in a simplified form. We consider that the virtual chains representing the surrounding phantom network and the entanglements are independent and can be superimposed to establish the measured net confinement

$$\frac{b_0^2}{\delta R_0^2} \approx \frac{f(f-2)\phi_0^{0.23}}{(f-1)N} + \frac{f\phi_0^\alpha}{2N_c(\phi_0 = 0.5)} \quad (10)$$

The first term refers to the swelling of the chains that enlarges cross-link displacements. The second term considers that the tube confinement of $f/2$ infinitely long chains is superimposed at an f -functional network junction,¹⁶ where $N_c(\phi_0 = 0.5)$ is the extrapolated entanglement constraint for “melt” conditions as in preceding simulations,¹⁶ and the ϕ_0^α term with an expected^{63,66} exponent of $\alpha \approx 1/(3\nu - 1) \approx 1.31$ explicitly models the concentration dependence of this constraint.

Preceding work¹⁶ used a more complex form of eq 10 based upon a recursion in order to consider also the entanglement constraints acting on the next generations of attached network junctions. For simplicity, here we have omitted these details. Omitting the recursion leads to a small overestimation for $N_c(\phi_0 = 0.5)$ when using $N_c(\phi_0 = 0.5)$ as an adjustable parameter. Recall that N_c describes the tube confining potential^{15,16} and not the entanglement degree of polymerization. The coefficient connecting N_c and N_c depends on the particular model for entangled polymers and must not be unity, see for example refs 8,16,59.

To reduce the number of adjustable parameters, we use the average number of elastically active branches per junction as the effective junction functionality of the networks at long times. This quantity is nearly constant for $\phi_0 N^{3\nu-1} \gtrsim 1$ and corresponds roughly to $f \approx 4w_{\text{act}} \approx 3.68$ for the corresponding samples. Figure 3 shows a reasonable agreement between the simulation data and eq 10 in the light of the approximations employed. For testing the exponent α , we have fitted the data for $N = 82$ using $N_c(\phi_0 = 0.5)$ and α as adjustable parameters providing $N_c(\phi_0 = 0.5) = 19.4 \pm 0.8$ and $\alpha = 1.35 \pm 0.07$. The exponent agrees with the theoretical prediction $\alpha \approx 1.31$ within the error bar. Our result for N_c exceeds the result of the preceding analysis¹⁶ only by about 20%, mainly due to omitting the recursion and since we used average data for chains between arbitrary star centers inside the elastically active material instead of focusing on connections

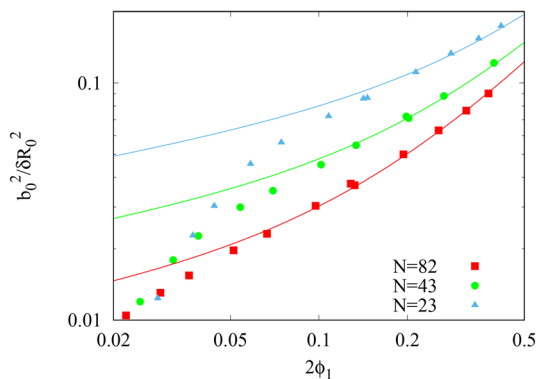


Figure 3. Inverse cross-link MSDs (Symbols). Data for $N = 82$ was fit with eq 10 providing $N_c(\phi_0 = 0.5) = 19.4 \pm 0.8$ and $\alpha = 1.35 \pm 0.07$. These parameters were kept fixed to plot the theoretical lines for $N < 82$.

between active junctions with four active connections. The assumption of a roughly constant N to model the phantom contribution breaks down in the vicinity of ϕ^* , leading to a reduced junction confinement. In the simulation data in Figure 3, this is at the point (roughly at $\phi_0 N^{3\nu-1} \approx 1$) where the data start to depart from the predicted behavior.

The expected change in the cross-link MSDs upon swelling is rather small. For the entanglement constraints, one expects a change of order $(\phi_0 Q)^{1/6}$, see eq 4, while the constraints arising from network connectivity (phantom modulus) grow $\propto (\phi_0 Q)^{0.23}$, see eqs 8 and 10. Altogether, a growth with an effective power in the range of 0.2 is expected. Indeed, our data in Figure 4 fit a power-law with a slightly larger exponent. This

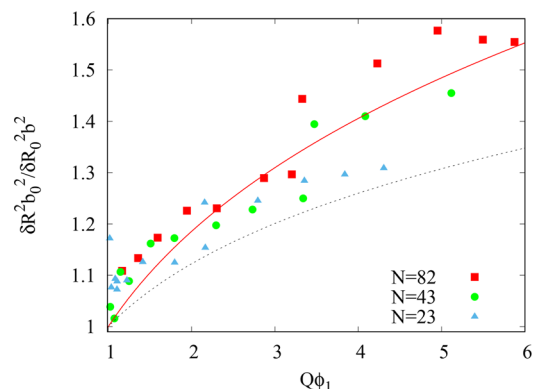


Figure 4. Ratio between the cross-link MSDs at swelling equilibrium and at preparation conditions. The continuous line is a fit using $(\phi_1 Q)^\beta$ with $\beta \approx 0.25 \pm 0.01$, the dashed lines shows $(\phi_1 Q)^{1/6}$ for comparison.

deviation is caused by the larger MSDs of the cross-links near the sample boundary: their impact propagates inward and is more pronounced in the set of samples that was prepared in the smaller box (the transition between both data sets is clearly visible by the vertical jump of the data for a given N at nearly the same ϕ_0). Therefore, the result for the exponent β in Figure 4 is an upper bound for the true change in the cross-link MSDs upon swelling. Thus, the swelling of the MSDs of cross-links is subaffine, $\beta < 1/3$, as expected theoretically.

Altogether, our results demonstrate that swelling of weakly entangled networks is well approximated by an affine deformation process. In section 5, we use this observation to

derive scaling relations connecting preparation conditions with the swollen state.

4. PREPARATION CONDITIONS

Let us consider model networks with a monodisperse distribution of the molar mass between the network junctions at a high conversion $p \approx 1$. As most polymers have no director along the chain segments, experimental NMR data is typically analyzed using the residual dipolar coupling that is proportional to the tensor order parameter S . The tensor order parameter is given by

$$S = \frac{1}{2}[(3\langle \cos^2 \theta \rangle) - 1] \quad (11)$$

Here, θ is the angle between \mathbf{R} and the instantaneous orientation of a chain segment, $\langle \dots \rangle$ denotes a time average of all conformations of a single chain, while $[\dots]$ denotes a sample average. The computation of scaling relations for the tensor order parameter is based upon²⁸

$$S \approx \frac{1}{15} \left[\beta_0 \left(\frac{R}{bN} \right)^{\nu/(1-\nu)} \right]^2 \quad (12)$$

that we present here in a simplified form ignoring corrections to scaling. β_0 is a constant that depends on the scaling of chain conformations, and b is the root-mean-square size of a Kuhn segment. There is $\beta_0 = 3$ for ideal chains with $\nu = 1/2$. For isolated chains, the term in the $[\dots]$ brackets is proportional to the force acting on the chain. In ref 28 eq 12 was tested explicitly with computer simulation data for swollen chains in the stretching limit, $\langle R \rangle > bN^\nu$, where the tension blobs become smaller than the size of the swollen coil. For smaller deformations, $\langle R \rangle < bN^\nu$, the deformation behavior of the chains is linear with the force.^{68,69} This latter regime refers to the situation where the tension blob size surpasses the chain size (for single chain deformation) and thus, the correlation length of the chain.

For nearly ideal polymer networks (or gels), the network defects establish only the minority of the network volume. In such systems, the correlation length (the length scale of excluded volume repulsion) cannot significantly exceed the size of a tension blob (the length scale of the elastic restoring forces). Both are essentially equivalent at swelling equilibrium⁵ whereby the correlation length decreases while the tension blobs grow upon drying the sample.⁶³ Both preparation state and equilibrium swelling refer, therefore, to the weak deformation limit with a linear relation between force and time-averaged size of the chains (the exponent inside the square brackets of eq 12 is unity). This was first demonstrated in ref 70 where it was found that $S \propto R^2/N^2$.

The vector order parameter m of a given Kuhn segment in a polymer is given by the time-averaged orientation of this bond vector. In the absence of entanglements and excluded volume interactions, one obtains^{15,71}

$$m = \frac{\langle R_{el} \rangle^2}{b^2 N_{el}^2} \quad (13)$$

Here, R_{el} is the end-to-end vector of an elastic chain with N_{el} segments. Combining this with eq 12, we obtain

$$S \approx \frac{3}{5} m \quad (14)$$

up to numerical corrections for scaling. We expect that this equation holds for nearly ideal networks in the preparation state and at swelling equilibrium since the tension blobs remain larger or equal to the correlation length as discussed above. As the vector order parameter m is simpler to compute, we focus on expressions for m in our discussion below.

The modulus of a sample determines the volume that stores an elastic energy equivalent to the thermal energy $k_B T$, where k_B is the Boltzmann constant and T the absolute temperature. In practice, this volume is converted into an effective elastic strand containing N_{el} Kuhn segments by use of the affine network model prediction for modulus

$$G_0 = \frac{k_B T}{v_K N_{el}} \phi_0 \quad (15)$$

Within the framework of the affine network model, one identifies a network strand with an elastic contribution of $k_B T$, that is $N_{el} = N$, whereby the chain ends are considered to be fixed in space. In the phantom network model, the restrictions for the network junctions arise from network connectivity, with corrections mainly related to the conformation in which the chain is linked to the network.²⁴ For our scaling analysis below, we skip these details as long as they concern only the coefficient relating the phantom modulus prediction with the affine model prediction. Significant corrections to scaling may arise for large amounts of inactive material, see section “swelling equilibrium” in ref 72, since network defects contribute to the osmotic pressure but not to modulus. As a benchmark for mapping the phantom model onto the affine model, we quote here only the result for perfect networks without finite loops where all junctions have exactly f connections to other junctions:

$$N_{el} = \frac{f}{f-2} N \quad (16)$$

For entangled networks, the elastic strand is the number of segments contributing $k_B T$ to modulus. It is expected that the deformation of the network strands turns into an affine deformation for chain sections containing N_{el} segments.⁸ Recall also that our analysis has shown that swelling is well approximated by an affine deformation of the elastic strands. Therefore, we simply consider strands of N_{el} segments as basic elastic units of the network, and we assume that deformation on the length scale of these strands is affine. Below, we keep in mind that $N_{el} \neq N$ and depends on the model of rubber elasticity. This is expressed in the equations by using N_{el} instead of N where appropriate.

At preparation conditions, the ensemble average end-to-end distance of a network strand is a function of the solvent quality and the polymer volume fraction. Approximately ideal chain conformations

$$R_0 \approx b N^{1/2} \quad (17)$$

independent of ϕ_0 are observed within the concentrated regime covering polymer volume fractions $\phi > \phi^{**}$. Within the good-solvent regime, $\phi^* < \phi_0 < \phi^{**}$, the chain size is a function of the polymer volume fraction,⁶⁴

$$\begin{aligned} R_0 &\approx \left(\frac{v}{v_K \phi_0} \right)^{(\nu-1/2)/(3\nu-1)} b N_{el}^{1/2} \\ &\approx \left(\frac{\phi^{**}}{\phi_0} \right)^{(\nu-1/2)/(3\nu-1)} b N^{1/2} \propto \phi_0^{-0.12} \end{aligned} \quad (18)$$

When averaging m in eq 13 over a large ensemble of chains with end-to-end distances R_{el} with approximately random walk statistics, one obtains for the concentrated regime, $\phi_0 > \phi^{**}$, that

$$[\langle R_0 \rangle^2] \approx b^2 N_{el} \quad (19)$$

Combining this average with eq 13 leads to

$$m_0 \approx \frac{1}{N_{el}} \quad (20)$$

Thus, at preparation conditions $\phi_0 > \phi^{**}$, modulus and the order parameter are related by

$$G_0 \approx \frac{k_B T}{v_K} m_0 \phi_0 \quad (21)$$

Note that the corrections to the scaling of chain conformations lead here also to a coefficient of order unity connecting the modulus with the order parameter.¹⁵

In the semidilute regime, $\phi^* < \phi_0 < \phi^{**}$, we expect an order parameter of

$$\begin{aligned} m_0 &\approx \frac{[\langle R_0 \rangle^2]}{b^2 N_{el}^2} \\ &\approx \left(\frac{v}{v_K \phi_0} \right)^{(2\nu-1)/(3\nu-1)} N_{el}^{-1} \propto \left(\frac{\phi_0}{\phi^{**}} \right)^{-0.23} N_{el}^{-1} \end{aligned} \quad (22)$$

related to modulus at preparation conditions via a slightly stronger dependence on ϕ_0 ,

$$\begin{aligned} G_0 &\approx \frac{k_B T}{v_K} m_0 \phi_0 \left(\frac{\phi_0}{\phi^{**}} \right)^{(2\nu-1)/(3\nu-1)} \\ &\approx \frac{k_B T}{v_K} m_0 \phi_0^{(5\nu-2)/(3\nu-1)} (\phi^{**})^{-(2\nu-1)/(3\nu-1)} \propto m_0 \phi_0^{1.23} \end{aligned} \quad (23)$$

The equations above define the basic relations between modulus, order parameter, and the preparation conditions that can be tested by computer simulations and in experiments. Indeed, a weak negative power-law for the concentration dependence of the order parameter m_0 is found in the simulations at intermediate concentrations, see Figure 5. The absolute of the exponent is smaller than predicted due to corrections in modulus, which grow weakly with the number fraction of $I_2 R_2$ in the system, as discussed in the preceding section. The point $\phi_0 N^{3\nu-1} \approx 1$ is roughly at the place where the data drop from this power-law toward small ϕ_0 , whereas for the largest ϕ_0 , there is either the predicted saturation of m_0 visible for $\phi_0 \gtrsim \phi^{**}$ or even a small increase, indicating the onset of entanglement effects on the residual bond orientations.

For experimental data, we expect further corrections to the behavior observed in Figure 5. As discussed in the preceding sections, we expect that conversion of the reactive groups grows

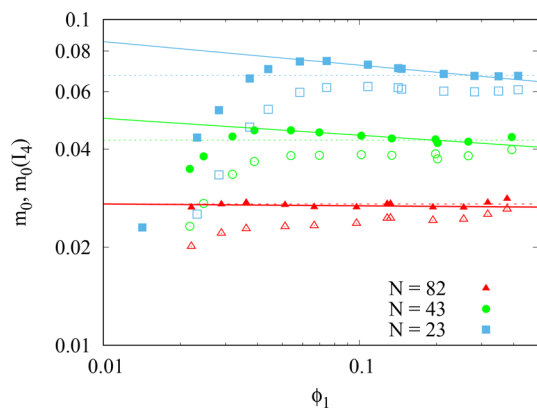


Figure 5. Sample averaged order parameter m_0 (open symbols) and the order parameter of the “ideal” connections $m_0(I)$ (full symbols) as a function of ϕ_0 . The dashed lines indicate a constant level of m_0 for comparison, the continuous line is a power-law fit to the $m_0(I)$ data at intermediate ϕ_0 leading to small negative powers between -0.07 and 0 .

weakly with ϕ_0 . Together with a reduction of R_2I_2 and an increase of I_4 for growing ϕ_0 , this leads to a modulus that grows faster than $\propto \phi$ even in the absence of a dominating contribution of entanglements. In fact, experimental studies⁷³ find that moduli of the corresponding tetra-PEG gels grow with an apparent power of approximately 1.3 as a function of ϕ_0 somewhat above the overlap concentration. Our rheology data in Figure 6 for a similar concentration range (c^* is here around

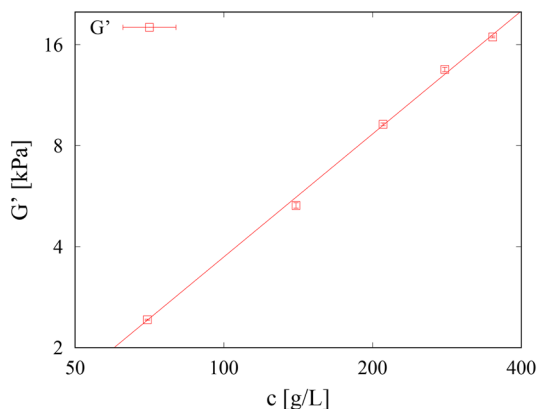


Figure 6. Experimental data for the storage modulus of as-prepared gels synthesized at different polymer concentrations.

60 g/L) fits to an exponent of 1.22 ± 0.05 , in good agreement with ref 73. This turns the predicted weak negative power of -0.23 for the residual bond orientation effectively into a nearly constant or weakly increasing behavior. In fact, a small positive power of 0.07 was found in literature²⁰ for ideal connections (“single links”) inside tetra PEG gels.

We have analyzed the residual dipolar coupling, D_{res} , with MQ-NMR for two sets of experiments that refer to different preparation conditions in the concentration range, see Figure 7. Analysis and sample preparation are described in detail in ref 30. Note that D_{res} is proportional to the tensor and the vector order parameter.^{71,74} The data carry a significant error, but fit best to a concentration independent behavior. Altogether, these observations support eq 23 for the good-solvent regime.

Finally, the samples with the largest N at the largest ϕ_0 in Figure 5 show a weak deviation toward larger residual bond

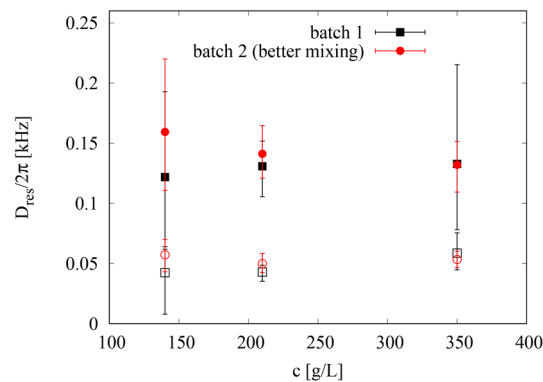


Figure 7. Experimental data for the residual bond order in terms of D_{res} , in the preparation state for two series of networks prepared in deuterated toluene. Full symbols refer to ideal connections, open symbols are double links.

orientations, which we attribute to the onset of entanglement effects. For entangled systems, it is expected^{15,75} that $m \propto (NN_e)^{-1/2}$, where N_e is the entanglement degree of polymerization (in numbers of Kuhn segments) in a melt of long chains of the same polymer. This scaling is derived using the “return-to-origin hypothesis”.⁷⁶ N_e is expected to grow with dilution $\propto \phi^{-4/3}$ in the concentrated regime and $\propto \phi^{-1/(3\nu-1)}$ in the semidilute regime.⁶³ Therefore, we expect

$$m \approx \phi_0^{2/3} (NN_e)^{-1/2} \quad (24)$$

in the entangled concentrated regime, while

$$m \approx \left(\frac{\phi^{**}}{\phi_0} \right)^{(2\nu-1)/(3\nu-1)} \phi_0^{-1/(6\nu-2)} (NN_e)^{-1/2} \quad (25)$$

is our expectation for the entangled semidilute regime. Note that N instead of N_e must be used here, since the N -dependence of m arises from the longitudinal motion of the chain segments along the confining tube.

Altogether, the available experimental data and our simulations support the proposed scaling model of residual bond orientations in the preparation state. The residual bond orientation is proportional to modulus, $G \propto m$, with $G \propto \phi_0$ and $G \propto \phi^{1.23}$ for the concentrated and the good-solvent regimes, respectively. These relations can be used to perform a first analysis of the concentration dependence of the modulus in the preparation state by NMR or computer simulations if a direct measurement of modulus is difficult. The results of this section are now combined with the scaling model of swelling equilibrium⁵ to provide scaling relations for the swollen state.

5. EQUILIBRIUM SWELLING

Swelling equilibrium is characterized by a balance of osmotic and elastic contributions to the free energy. Thus, the modulus of the gel at swelling equilibrium, G , is equivalent to the osmotic pressure kT/ξ^3 at this polymer volume fraction. The osmotic pressure is only a function of ϕ and determines the modulus at swelling equilibrium⁵

$$G \approx \frac{k_B T}{v_K} \begin{cases} \left(\frac{v}{v_K}\right)^{(6\nu-3)/(3\nu-1)} \phi^{3\nu/(3\nu-1)} & \text{good solvent} \\ \phi^3 & \theta - \text{solvent} \end{cases} \quad (26)$$

This general result holds independently of network architecture or preparation conditions, and it is the key to understand the elastic properties at swelling equilibrium. Recall that the athermal limit is obtained for $\nu \approx b^3$.

The different scaling of chain conformations within the semidilute and the concentrated regimes leads to two different scaling regimes for the modulus. The concentration dependence of the modulus is best discussed by generalizing eq 15 to the Panyukov form

$$G_{\text{ph}}(\phi) \approx \frac{\phi k_B T}{v_K N_{\text{el}}} \left(\frac{\lambda R_0}{R_{\text{ref}}}\right)^2 \quad (27)$$

Here, R_0 is the undeformed reference size of the chain at preparation conditions, and λ describes the deformation of the chains with respect to R_0 . R_{ref} is the reference chain size of a polymer chain in a polymer solution with the same solvent at a polymer volume fraction ϕ . It is given by inserting ϕ instead of ϕ_0 into eq 18, if $\phi < \phi^{**}$, while it is ideal otherwise.

The different scaling regimes of R_{ref} and R_0 imply that we have to discuss three different cases:

- Swelling in theta solvent, $\phi^{**} < \phi < \phi_0$, where both R_{ref} and R_0 remain nearly ideal,
- the “intermediate” case $\phi < \phi^{**} < \phi_0$ where R_{ref} refers to swollen chains, while R_0 remains ideal, and
- swelling in a good solvent $\phi < \phi_0 < \phi^{**}$ where both R_{ref} and R_0 refer to the swollen chain conformations.

The Appendix contains a complete discussion and derivation of the results including analytical expressions for all exponents. Below, we summarize these computations in compact form for all three regimes providing numerical exponents based upon $\nu \approx 0.5876$ for good solvent for convenience.

From top to bottom in each equation, the results refer to cases (a–c) above. The modulus as a function of polymer volume fraction scales as

$$G(\phi) \approx \frac{k_B T}{v_K N_{\text{el}}} \begin{cases} \phi_0^{2/3} \phi^{1/3} \\ \phi_0^{2/3} \phi^{0.56} (\phi^{**})^{-0.23} \\ \phi_0^{0.44} \phi^{0.56} \end{cases} \quad (28)$$

the equilibrium degree of swelling is approximately

$$Q \approx \begin{cases} N_{\text{el}}^{3/8} \phi_0^{-1/4} \\ N_{\text{el}}^{0.57} \phi_0^{-0.38} (\phi^{**})^{0.69} \\ N_{\text{el}}^{0.57} \phi_0^{-1/4} (\phi^{**})^{0.39} \end{cases} \quad (29)$$

whereas the vector order parameter as a function of polymer volume fraction is

$$m(\phi) \approx \frac{1}{N_{\text{el}}} \begin{cases} \phi_0^{2/3} \phi^{-2/3} \\ \phi_0^{2/3} \phi^{-2/3} \\ \phi_0^{0.44} (\phi^{**})^{0.23} \phi^{-2/3} \end{cases} \quad (30)$$

At swelling equilibrium, the vector order parameter becomes

$$m \approx \begin{cases} N_{\text{el}}^{-3/4} \phi_0^{1/2} \\ N_{\text{el}}^{-0.62} \phi_0^{0.41} (\phi^{**})^{0.35} \\ N_{\text{el}}^{-0.62} \phi_0^{0.27} (\phi^{**})^{0.49} \end{cases} \quad (31)$$

which can be expressed as a function of the equilibrium degree of swelling

$$m \approx \begin{cases} Q^{-2} \\ (\phi^{**})^{0.92} Q^{-1.08} \\ (\phi^{**})^{0.92} Q^{-1.08} \end{cases} \quad (32)$$

and leads to a relation between order parameter and modulus at swelling equilibrium

$$G \approx \frac{k_B T}{v_K} \begin{cases} m^{3/2} \\ m^{2.14} (\phi^{**})^{-1.28} \\ m^{2.14} (\phi^{**})^{-1.28} \end{cases} \quad (33)$$

The first two of these equations have been derived first in ref.⁵ while the rest are new results of this work.

The equilibrium degree of swelling, Q , as a function of ϕ_0 is shown in Figure 8. We have scaled the concentration axis by

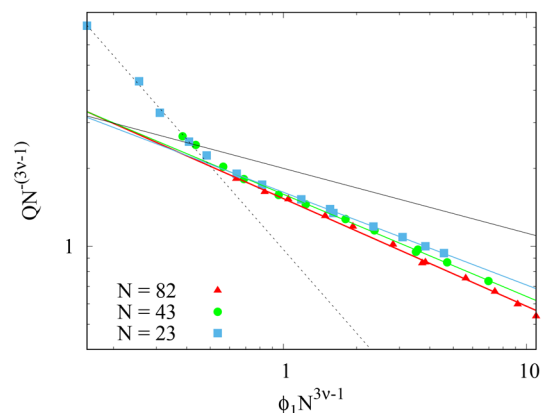


Figure 8. Equilibrium degree of swelling, Q , as a function of the polymer volume fraction at preparation conditions, ϕ_0 . The continuous lines are fits of the data with a power-law decay $Q \propto \phi_0^{-\gamma}$ providing an effective exponent $\gamma = 0.36 \pm 0.01$ for $N = 23$, $\gamma = 0.39 \pm 0.01$ for $N = 43$, and $\gamma = 0.42 \pm 0.01$ for $N = 82$. The dashed line is a power-law $\phi_0^{-1.07}$ and the thin black continuous line indicates a power-law with $\gamma = -1/4$.

$N^{(3\nu-1)}$ and normalized swelling by the scaling of the swelling degree of networks strands at ϕ^* . This produces a collapse of the data around the overlap concentration and below, while the data above this threshold follows slightly different apparent power-laws with a weakly increasing power γ for larger N . Our simulations refer to swelling in the good-solvent regime. According to eq 29, we would expect $Q \propto \phi_0^{-1/4}$ for our data.

For entangled systems, one could expect that the equilibrium degree of swelling is reached if the swollen affine strands are at overlap, enforcing des-interspersion of temporary entanglements on a smaller scale. This situation would refer to a scaling

$$Q \approx N_e(\phi_0)^{(3\nu-1)} \propto (N_e\phi_0^{-1/(3\nu-1)})^{(3\nu-1)} \propto \phi_0^{-1} \quad (34)$$

which is clearly a stronger dependence on ϕ_0 as compared to the entanglement free limit. The trend of our data for increasing N does not contradict such a scaling limit. However, due to the slowly changing power it is questionable whether this asymptotic scaling can be reached within the experimentally accessible range of N .

The final and most universal test of our scaling relations for the residual bond orientation is given in Figure 9, where the

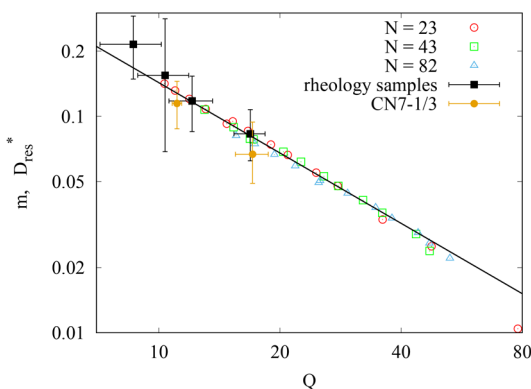


Figure 9. Average order parameter m in the simulations (open symbols) and residual dipolar coupling of the experiments (full symbols) as a function of the equilibrium degree of swelling, Q . The line shows the predicted scaling of $m = cQ^{-1.08}$ with coefficient $c = 0.81 \pm 0.01$ as the only adjustable parameter to fit the simulation data. The numerical error of the simulation data is comparable to symbol size. D_{res}^* is the residual dipolar coupling of the experiments multiplied by a numerical factor to obtain overlap with m in the plot. The “rheology samples” are the samples of Figure 6 except for one that was damaged during transport. Samples CN7–1/3 are charge 7 or ref 30 at concentrations of roughly c^* and $3c^*$.

vector order parameter is shown as a function of the equilibrium degree of swelling. In this plot, subtle points of the dependence of Q on ϕ_0 become irrelevant as corrections to modulus are compensated through the swelling equilibrium by plotting the data as a function of Q . The collapse of the simulation data and the agreement with the predicted scaling speaks for itself. The figure also contains data for MQ-based residual dipolar couplings that were scaled to overlap with m . The experimental data carries a considerable uncertainty but fits qualitatively to the simulation data at large Q . Recall that conversion is not constant for the experimental data. Therefore, we expect a somewhat stronger decay as a function of Q similar to the trend of the simulation data at the largest Q , where cyclic defects impact the scaling.

6. DISCUSSION

The results of the above sections provide additional insights when compared with preceding work in literature. In ref 70, it was shown that the residual bond orientation decreases for low degrees of swelling before it runs through a minimum and starts to rise in a nearly affine fashion toward swelling equilibrium. This observation was confirmed in subsequent work.^{28,77}

Various explanations for this effect have been discussed including swelling heterogeneities⁷⁸ or a possible release of topological constraints due to swelling.⁷⁰ In Figure 4, we have shown that the cross-link MSDs grow slowly with the (equilibrium) degree of swelling $\propto (\phi_0 Q)^\beta$, with an exponent that should not exceed $\beta \approx 0.25$. Clearly, the affine and phantom models of rubber elasticity provide no possibility to explain this behavior. In the framework of the constrained junction model, we may approximate for the swelling process that

$$m = \frac{R^2}{b^2 N_{\text{comb}}} \approx \frac{(\phi_0 Q)^{2/3}}{b^2 [N + 2n_0(\phi_0 Q)^\beta]} \quad (35)$$

Here, n_0 is the degree of polymerization of the virtual chain that describes the cross-link fluctuations (after disconnecting the N -mer between) in the preparation state. N_{comb} is the effective combined chain made of the two virtual chains to the nonfluctuating elastic background. This combined chain grows with dilution approximately like $N_{\text{comb}} \approx N + 2n_0(\phi_0 Q)^\beta$. Since $dm/dQ > 0$ for all N and n_0 , a release of the constraints acting on the network junctions alone cannot explain the observation of a minimum. A similar reasoning for entangled chains arrives at the same qualitative result. Thus, the minimum of the residual dipolar coupling requires an additional explanation like a des-interspersion process of chains or a rearrangement of the confining tubes, unless this observation is caused by an incomplete averaging of the segment orientations⁷⁹ at high polymer volume fractions.

An observation made in this context was the shift and an apparent broadening of the distribution of the segment orientations during swelling.⁷⁸ In order to test whether such a broadening occurs or not, we plot in Figure 10 the residual bond

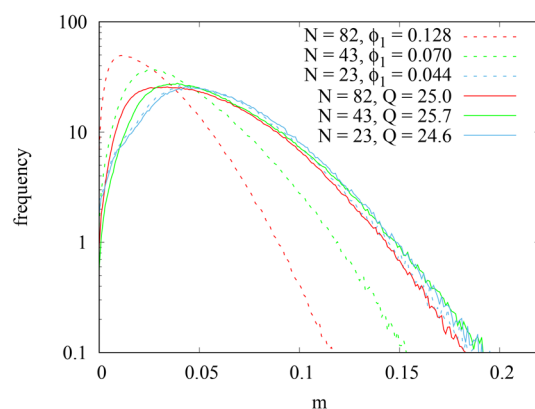


Figure 10. Comparison of the normalized distribution of the residual bond orientations at preparation conditions (dashed lines) and at equilibrium swelling (continuous lines).

orientations of the elastically active segments for three samples with an almost identical equilibrium degree of swelling. The distributions of the order parameters of the three swollen samples essentially fall on top of each other, except for a small difference at the left flank of the peak. This difference is caused by the correlation hole of the star centers, which is a function of the overlap of the stars at preparation conditions^{27,51,80} causing a stronger depletion of the shortest end-to-end distances the smaller the overlap of the star polymers at preparation. Except for this detail, there is no systematic broadening of the distributions at the same degree of swelling. This means that an apparent broadening (when changing from preparation

conditions to equilibrium swelling) actually results from a contraction of the distribution toward the preparation state. Such a behavior was predicted for entangled networks,^{15,75} where the contraction results from the longitudinal Rouse modes of the chain segments along the confining tubes allowing the chain segments to sample tube sections with different orientations. Interestingly, there is no such contraction of the distributions in the swollen state, since the $N = 23$ sample was cross-linked at the overlap threshold and does not significantly increase Q upon swelling. This also means that these longitudinal Rouse modes must be damped out at swelling equilibrium for the samples with a larger N . This latter point fits well into the scaling picture proposed above: at swelling equilibrium, the size of a tension blob is the same as the correlation length. Thus, entangled chains at swelling equilibrium have reached a “fully stretched” state of correlation volumes, which damps out the longitudinal motion of the correlation volumes along the confining tube.

The three data sets in Figure 10 have approximately the same Q even though N differs by a factor of almost 4. Therefore, the c^* theorem proposed by De Gennes⁶⁴ cannot be correct. In the c^* theorem, it was conjectured that swelling equilibrium is reached after a full des-interpersation of the network strands removing all entanglements between the chains. Such a process would lead to an equilibrium degree of swelling of

$$Q^* = \frac{1}{\phi^*} \propto N^{3\nu-1} \quad (36)$$

with an equilibrium chain size of $R \approx bN^\nu$ in good solvents at swelling equilibrium, independent of preparation conditions. Since the tension blob is then not smaller than the correlation length, we can proceed as above. For the order parameter at swelling equilibrium we obtain that

$$m^* \approx \frac{R^2}{b^2 N^2} \approx N^{2\nu-2} \approx (Q^*)^{(2\nu-2)/(3\nu-1)} \quad (37)$$

which is exactly the same dependence derived using our scaling approach, see eq A21. The reason behind this equivalence is that in both cases one establishes an equilibrium between tension blobs and correlation volumes. The only “mistake” of the c^* theorem is to propose that this must occur at the length scale of the network strand, N , instead of the elastic strand inside the swollen system.

Previously, a different relation $S \propto Q^{-1.5}$ was considered to support the c^* theorem.⁸¹ Another theoretical work²⁸ derived a similar relation $S \propto Q_s^{-1.46}$ where $Q_s = V/V_0$ was defined with respect to preparation conditions instead of the dry state. Interestingly, both works came – as we do – with their personal set of data, supporting their theory. A dependence of $\propto Q_s^{-x}$ translates into a proportionality $\propto (\phi_0 Q)^{-x}$, since $\phi_0 = V_{\text{dry}}/V_0$. Thus, the observed scaling is not universal in Q due to the additional dependence on ϕ_0 . However, modulus at swelling equilibrium must be a universal function of Q independent of preparation conditions, since modulus compensates the osmotic pressure, see eq 26. Moreover, the segment orientations are also a universal function of Q , since the segment orientations are dominated by the properties of the tension blobs, which scale universally with the modulus. This universality is satisfied in our approach, see eq 32, but not in ref 28.

An observation of $S \propto Q^{-1.5}$ in an experiment, however,⁸¹ can stem from several reasons (or a combination of these). First, there might be a crossover from theta to good-solvent conditions

when small Q are involved, leading to an effective power intermediate between -2 for theta solvents and -1.08 for the good-solvent limit. For randomly cross-linked networks prepared at the same polymer volume fraction, one obtains a larger degree of swelling by reducing the density of cross-links. For a random cross-linking process, this is equivalent to increasing the weight fraction of pending chains,^{54,82} thus reducing in turn the weight fraction of the elastically active material, w_{act} . The series of networks with $N = 23$ contains extra data points for which w_{act} is significantly decreasing with decreasing ϕ_0 . A power-law fit to the four data points with $w_{\text{act}} < 0.9$ leads to an effective power of -1.35 ± 0.1 , significantly closer to the scaling observed in ref 81. This demonstrates that a consideration of network defects is crucial for discussing data on equilibrium swelling.^{72,79} This proves the advantage of using model architectures like heterocomplementary coupled stars to test and to develop theory.

7. SUMMARY

We have presented large-scale computer simulations and experimental data on the equilibrium swelling of model networks and compared these with a new scaling model of the residual bond orientations in swollen networks. Networks were prepared using a heterocomplementary coupling of star polymers to suppress the formation of pending loops. Solutions of four-arm star polymers were prepared at different volume fractions of the polymer, and for the simulations also with different degrees of polymerization of the star polymers. The analysis of network structure showed that only minor corrections to scaling can be expected when focusing on networks beyond overlap of the stars, $\phi_0 N^{3\nu-1} > 1$. In the simulations, the affinity of the swelling process was analyzed based upon time-averaged chain conformations. This analysis revealed only minor deviations from an affine swelling process. These deviations grow with the overlap number of the star polymers at preparation conditions, hinting toward entanglements as the possible origin. From a theoretical perspective, scaling relations were derived for the residual bond orientation at preparation conditions and at equilibrium swelling. The prediction $G_0 \propto m_0 \phi_0^{1.23}$ at preparation conditions relates modulus at preparation conditions, G_0 , with the residual bond orientation, m_0 , and the change in the equilibrium chain conformations at preparation conditions. This prediction agrees with our experimental data and preceding work. For swelling in theta solvents, we predict that $m \propto Q^{-2}$ and $G \propto m^{3/2}$. Upon the basis of the same principles, we derived that $m \propto Q^{-1.08}$ with $G \propto m^{2.14}$ in the good-solvent regime. All results at swelling equilibrium are predicted to remain independent of preparation conditions. The agreement of our simulation data with the scaling relation $m \propto Q^{-1.08}$ is superb. Our set of experimental data supports this scaling relation as well. Together with the known scaling relations for modulus at swelling equilibrium, this agreement strongly supports our model. However, our simulation data show also that significant corrections to scaling may arise in networks with a less well-defined structure containing a larger fraction of defects.

APPENDIX

Throughout the Appendix, we use definitions and terms as introduced in the main text. In the first subsection, we provide additional information on the analysis of the simulation data. The following three subsections contain the explicit derivation

of the scaling results that were presented in simplified form in Section 5 of the main part of this work. The last part of the Appendix describes the model predictions in case of an affine deswelling.

A. Analysis of Simulation Data

The average residual bond orientation is analyzed by extrapolation towards infinite time as introduced in ref 51. Let t be the number of the sample snapshots ($t = 1, 2, \dots$). The running average of the residual bond orientations of a certain class of chain segments is computed from the average coordinates of the monomers up to snapshot t as described in ref 15. These data are plotted vs $1/t$ and extrapolated towards $t \rightarrow \infty$, as shown in Figure A1.

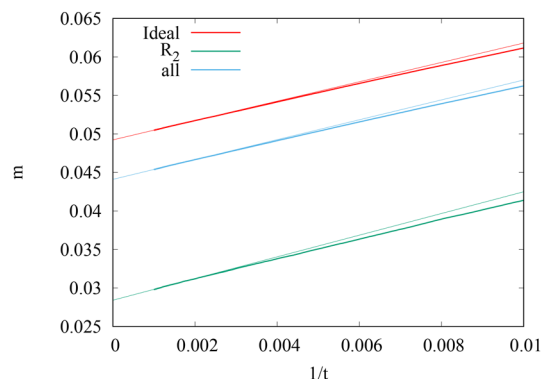


Figure A1. Extrapolation of the residual bond orientations of the network with $N = 82$, $L = 512$, and $M = 9600$ in the swollen state. Data concern either all segments, the segments within “ideal” connections inside the elastically active material, or the segments in R_2 loops.

The equilibrium degree of swelling, Q , and the effective volume fraction inside the preparation box, ϕ_1 , were determined using the following algorithm. From each snapshot of the sample, linear volume fraction profiles of the swollen gel are computed in each direction. Then, for each direction the following steps are performed independently in all directions: (1) the average polymer volume fraction is computed inside the simulation box (2) then from all six sides of the simulation box inwards, the position is determined at which this average level is surpassed for the first time. (3) These positions are used to define a smaller box for which the average polymer volume fraction is computed. (4) Step 2 and 3 are repeated twice, but now each time searching for the point where 90% of the average density are reached for defining the boundary.

We have checked with randomly selected snapshots of the volume fraction profile that the above algorithm converges towards a reasonable description of the polymer volume fraction inside the sample. Figure A2 contains one example where the “last” box of the above algorithm is shown together with the estimate of the average volume fraction along a particular axis of the sample (the true volume fraction inside the “last” box is significantly larger since the boundary zones are cut in each direction). The polymer volume fraction in the last box of swollen systems is used to compute an estimate of Q (or of ϕ_1) with respect to $\phi = 1$. The equilibrium degree of swelling Q is shown in Figure A3 as a function of the snapshot number t . Except for increasing noise in samples with larger equilibrium degree of swelling, there is no systematic drift of Q as a function of t for all samples, indicating sufficient equilibration of the samples prior to measurement.

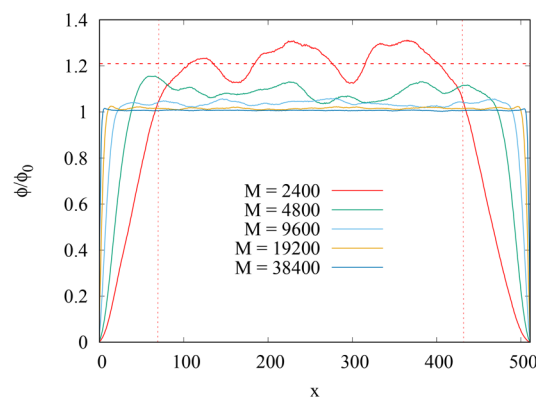


Figure A2. One-dimensional volume fraction profile in the full box along the x -axis of the as-prepared gels at low polymer volume fraction with $N = 43$ and $L = 512$. All profiles are averages over all 1000 snapshots of the sample. The vertical lines indicate the dimension of the “last” box for analyzing ϕ_1 (the dashed horizontal line for the preparation state of the sample with $M = 2400$).

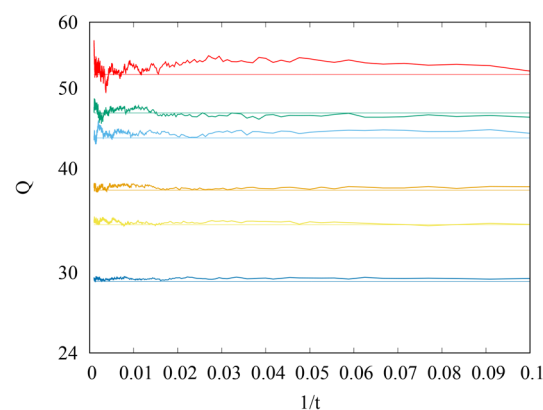


Figure A3. Equilibrium degree of swelling, Q , as a function of the number of the snapshot t (taken every 10^5 MCS) after equilibration. Data for samples with $N = 82$ and $L = 512$. Lines refer to $M = 1600, 2400, 3200, 4800, 6400,$ and 9600 (from top to bottom). Horizontal lines show the average Q of all snapshots.

For swollen systems, drift and rotation of the full sample were subtracted in the following way. First, at preparation conditions, the elastically active cross-links within the lowest 64 and the highest 64 lattice layers in each direction were marked providing 6 sets of marked cross-links where cross-links next to corners of the sample show up in three sets simultaneously. For each snapshot of the swollen system, the center of mass of the active network was determined, and all coordinates were computed with respect to this center of mass. Next, the centers of mass of each of the six sets of marked cross-links are computed. These latter coordinates are used to compute orientation vectors in each spatial direction. Then, the ortho-normal basis with the smallest angular difference to these orientation vectors is computed. Finally, all coordinates of the swollen system are expressed using this coordinate system for analyzing \bar{R}^2 and δR^2 in the swollen state. Without these corrections, δR^2 is significantly overestimated for the smallest samples due to the very long simulation runs of our study. The same analysis was applied for the preparation state in order to avoid a systematic bias due to a different data treatment.

B. Swelling in Theta Solvents and within the Concentrated Regime, $\phi^{**} < \phi < \phi_0$

Here, both R_{ref} and R_0 remain ideal, see eq 17. Therefore, from eq 26 one obtains

$$G(\phi) \approx \frac{\phi k_B T}{v_K N_{\text{el}}} \lambda^2 \approx \frac{k_B T}{v_K N_{\text{el}}} \phi_0^{2/3} \phi^{1/3} \quad (\text{A1})$$

Within the affine approximation of swelling, the squared chain size is stretched by a factor of λ^2 , providing

$$m(\phi) \approx \frac{R^2}{b^2 N_{\text{el}}^2} \approx \frac{\lambda^2 R_0^2}{b^2 N_{\text{el}}^2} \approx \left(\frac{\phi_0}{\phi} \right)^{2/3} N_{\text{el}}^{-1} \quad (\text{A2})$$

Swelling equilibrium is found by balancing modulus with osmotic pressure, see eq 26, giving an equilibrium degree of swelling⁵ of

$$Q = \frac{1}{\phi} \approx N_{\text{el}}^{3/8} \phi_0^{-1/4} \quad (\text{A3})$$

Therefore, the order parameter at swelling equilibrium reads

$$m \approx (\phi_0 N_{\text{el}}^{3/8} \phi_0^{-1/4})^{2/3} N_{\text{el}}^{-1} \approx N_{\text{el}}^{-3/4} \phi_0^{1/2} \quad (\text{A4})$$

This relation can be expressed as a function of Q after solving eq A3 for N_{el}

$$m \approx Q^{-2} \quad (\text{A5})$$

The result is independent of preparation conditions and network architecture, similar to the general expression for modulus at swelling equilibrium, eq 26. The latter can be written as a function of the equilibrium degree of swelling

$$G \approx \frac{k_B T}{v_K} Q^{-3} \quad (\text{A6})$$

Thus, in the concentrated regime, modulus and order parameter have a rather simple and general relation at swelling equilibrium

$$G \approx \frac{k_B T}{v_K Q^3} \approx \frac{k_B T}{v_K} m^{3/2} \quad (\text{A7})$$

C. Swelling in the Intermediate Regime, $\phi < \phi^{**} < \phi_0$

In this regime, chain size is ideal at preparation conditions and given by eq 17, while the reference chain size in the swelling equilibrium is swollen and follows eq 18 at polymer volume fraction ϕ . This leads to⁶³

$$\begin{aligned} G(\phi) &\approx \frac{\phi k_B T}{v_K N_{\text{el}}} \left(\frac{\lambda R_0}{R_{\text{ref}}} \right)^2 \\ &\approx \frac{\phi k_B T}{v_K N_{\text{el}}} \left(\frac{\phi_0}{\phi} \right)^{2/3} \left(\frac{\phi}{\phi^{**}} \right)^{(2\nu-1)/(3\nu-1)} \\ &\approx \frac{k_B T}{v_K N_{\text{el}}} \phi_0^{2/3} (\phi^{**})^{-(2\nu-1)/(3\nu-1)} \phi^{(9\nu-4)/(9\nu-3)} \end{aligned} \quad (\text{A8})$$

because of $\phi < \phi^{**}$. Since the final state is in the good-solvent regime, we balance this expression for modulus with the good-solvent branch of eq 26:

$$Q = \phi^{-1} \approx \left(\frac{N_{\text{el}}}{\phi_0^{2/3}} \right)^{(9\nu-3)/4} (\phi^{**})^{6\nu-3} \quad (\text{A9})$$

In practice, the equilibrium degree of swelling is often used to estimate the degree of polymerization of the elastic strand,

$$N_{\text{el}} \approx Q^{4/(9\nu-3)} (\phi^{**})^{-(8\nu-4)/(3\nu-1)} \phi_0^{2/3} \quad (\text{A10})$$

We assume that the deformation of the elastic strand is affine with the sample geometry starting from ideal chain conformations at preparation conditions $\phi_0 > \phi^{**}$. In swelling equilibrium, the vector order parameter becomes

$$\begin{aligned} m &\approx \left(\frac{\phi_0}{\phi} \right)^{2/3} N_{\text{el}}^{-1} \\ &\approx (\phi^{**})^{(4\nu-2)} \phi_0^{1-\nu} N_{\text{el}}^{(3\nu-3)/2} \end{aligned} \quad (\text{A11})$$

This result can be expressed as a function of the equilibrium degree of swelling using eq A10

$$\begin{aligned} m &\approx (\phi^{**})^{(8\nu-4)/(3\nu-1)} Q^{-(2-2\nu)/(3\nu-1)} \\ &\approx (\phi^{**})^{0.92} Q^{-1.08} \end{aligned} \quad (\text{A12})$$

which is independent of ϕ_0 but depends only on the solvent quality included in ϕ^{**} and on the equilibrium degree of swelling, Q .

The modulus at swelling equilibrium is written as a function of preparation conditions by inserting $\phi = Q^{-1}$ into the good-solvent branch of eq 26. This gives

$$\begin{aligned} G &\approx \frac{k_B T}{b^3} \left(\frac{v}{v_K} \right)^{(6\nu-3)/(3\nu-1)} Q^{-3\nu/(3\nu-1)} \\ &\approx \frac{k_B T}{v_K} \left(\frac{\phi_0^{2/3}}{N_{\text{el}}} \right)^{9\nu/4} (\phi^{**})^{-(6\nu-3)} \end{aligned} \quad (\text{A13})$$

Let us rearrange eq A12

$$Q^{-3\nu/(3\nu-1)} \approx m^{3\nu/(2\nu-2)} (\phi^{**})^{-3\nu(4\nu-2)/[(3\nu-1)(1-\nu)]}$$

and insert this relation into the above equation for G . This provides the missing relation between modulus and vector order parameter

$$\begin{aligned} G &\approx \frac{k_B T}{v_K} m^{3\nu/(2-2\nu)} (\phi^{**})^{-3(2\nu-1)/(1-\nu)} \\ &\approx \frac{k_B T}{v_K} m^{2.14} (\phi^{**})^{-1.28} \end{aligned} \quad (\text{A14})$$

D. Swelling in the Good-Solvent Regime, $\phi < \phi_0 < \phi^{**}$

In the good-solvent regime, the reference chain sizes in the swollen and preparation state, R_{ref} and R_0 , are described by eq 18. Using the same arguments as above, this leads to

$$\begin{aligned} G(\phi) &\approx \frac{\phi k_B T}{v_K N_{\text{el}}} \left(\frac{\lambda R_0}{R_{\text{ref}}} \right)^2 \\ &\approx \frac{\phi k_B T}{v_K N_{\text{el}}} \left(\frac{\phi_0}{\phi} \right)^{2/3} \left(\frac{\phi}{\phi_0} \right)^{(2\nu-1)/(3\nu-1)} \\ &\approx \frac{k_B T}{v_K N_{\text{el}}} \phi_0^{1/(9\nu-3)} \phi^{(9\nu-4)/(9\nu-3)} \end{aligned} \quad (\text{A15})$$

The above expression needs to match the osmotic pressure at equilibrium swelling in the good-solvent regime. Balancing the good-solvent branch of eq 26 with eq A15, one obtains

$$Q = \phi^{-1} \approx N_{\text{el}}^{(9\nu-3)/4} \phi_0^{-1/4} (\phi^{**})^{9(2\nu-1)/4} \quad (\text{A16})$$

As in the preceding cases, the degree of polymerization of the elastic strand can be estimated as

$$N_{\text{el}} \approx Q^{4/(9\nu-3)} \phi_0^{1/(9\nu-3)} (\phi^{**})^{-(6\nu-3)/(3\nu-1)} \quad (\text{A17})$$

The vector order parameter is only related to chain size at swelling equilibrium. We assume that the square chain size deforms affinely by a factor of λ^2 from preparation conditions:

$$R^2 \approx \lambda^2 R_0^2 \approx \left(\frac{\phi_0}{\phi}\right)^{2/3} \left(\frac{\phi^{**}}{\phi_0}\right)^{(2\nu-1)/(3\nu-1)} b^2 N_{\text{el}} \quad (\text{A18})$$

providing

$$\begin{aligned} m(\phi) &\approx \frac{R^2}{b^2 N_{\text{el}}} \\ &\approx \phi^{-2/3} \phi_0^{1/(9\nu-3)} (\phi^{**})^{(2\nu-1)/(3\nu-1)} N_{\text{el}}^{-1} \end{aligned} \quad (\text{A19})$$

At swelling equilibrium, $\phi = Q^{-1}$, this becomes

$$m \approx \phi_0^{(1-\nu)/(6\nu-2)} (\phi^{**})^{(2\nu-1)(9\nu-1)/(6\nu-2)} N_{\text{el}}^{-(3-3\nu)/2} \quad (\text{A20})$$

For expressing m as a function of Q , we insert eq A17 for N_{el} . This gives

$$\begin{aligned} m &\approx (\phi^{**})^{(8\nu-4)/(3\nu-1)} Q^{-(2-2\nu)/(3\nu-1)} \\ &\approx (\phi^{**})^{0.92} Q^{-1.08} \end{aligned} \quad (\text{A21})$$

which is again independent of preparation conditions, ϕ_0 . The dependence on Q is the same as in the intermediate case, only the dependence on ϕ^{**} is different, since now both preparation state and swelling equilibrium are below ϕ^{**} .

The relation between modulus at swelling equilibrium and preparation conditions is revealed by inserting $\phi = Q^{-1}$ into eq A15

$$\begin{aligned} G &\approx \frac{k_{\text{B}}T}{v_{\text{K}}} (\phi^{**})^{(6\nu-3)/(3\nu-1)} Q^{-3\nu/(3\nu-1)} \\ &\approx \frac{k_{\text{B}}T}{b^3} N_{\text{el}}^{-9\nu/4} \phi_0^{3\nu/(12\nu-4)} (\phi^{**})^{-(6\nu-3)(9\nu-4)/(12\nu-4)} \end{aligned} \quad (\text{A22})$$

Therefore, the relation between modulus and order parameter at swelling equilibrium is

$$\begin{aligned} G &\approx \frac{k_{\text{B}}T}{v_{\text{K}}} m^{3\nu/(2-2\nu)} (\phi^{**})^{-(6\nu-3)/(1-\nu)} \\ &\approx \frac{k_{\text{B}}T}{v_{\text{K}}} m^{2.14} (\phi^{**})^{-1.28} \end{aligned} \quad (\text{A23})$$

This is the same relation as for the intermediate case regarding the dependence on m , with a clearly stronger dependence on ϕ^{**} .

E. Dried Gels

Gels can be dried, and it is interesting to estimate the properties of the dry samples based upon the preparation conditions or swelling equilibrium. In this section, we provide the expected

scaling relations connecting modulus and the order parameter in the dry state with swelling equilibrium and preparation conditions. For this purpose, we assume that de-swelling or drying leads to an approximately affine displacement of the network junctions as in the preceding sections. We further discuss only the non-entangled limit. The opposite limit of entangled chains is more complex as the entanglement constraints come closer and lead to modified entanglement contributions to modulus depending on the model for the entangled chains, which is beyond our scope. The scaling relations below hold only for samples that remain mobile in the dried state and neither go through a glass transition nor crystallize.

Drying from Theta Solvents: $\phi^{**} < \phi < \phi_0$. Setting $\phi = 1$ in eq A1 and using eq A3 leads to

$$G_{\text{dry}} \approx \frac{k_{\text{B}}T}{N_{\text{el}} b^3} \phi_0^{2/3} \approx \frac{k_{\text{B}}T}{b^3} Q^{-8/3} \quad (\text{A24})$$

A similar reasoning applies for the order parameter of deswollen gels. Again, we use that m is proportional to the squared size of the elastic strands, which is assumed to deform affinely. Moreover, this provides for $\phi = 1$ a universal relation with the equilibrium degree of swelling

$$m_{\text{dry}} \approx \phi_0^{2/3} N_{\text{el}}^{-1} \approx Q^{-8/3} \quad (\text{A25})$$

Comparing with the expression for G_{dry} , we see that this relation is in accord with eq A7 for $\phi = 1$, suggesting that eq A7 holds for any intermediate degree of partial swelling and equilibrium degree of swelling as long as the samples remain within the concentrated regime or swell and dry with theta solvents.

Drying for the Intermediate Regime, $\phi < \phi^{**} < \phi_0$. The order parameter of the network at preparation conditions is given by eq 20. It decreases affinely with sample size upon drying, see the first part of eq A25, but in the intermediate regime, it develops a different relation with the equilibrium degree of swelling. Thus,

$$m_{\text{dry}} \approx \frac{\phi_0^{2/3}}{N_{\text{el}}} \approx Q^{-4/(9\nu-3)} (\phi^{**})^{(8\nu-4)/(3\nu-1)} \quad (\text{A26})$$

Similarly, the dry modulus depends on the preparation state as given by the first part of eq A24, while for relating G_{dry} with Q , we first insert eq A10 and recall that extrapolating modulus up to $\phi = 1$ along eq A8 underestimates dry modulus by a factor of $(\phi^{**})^{-(2\nu-1)/(3\nu-1)}$, since the reference chain size no more shrinks for $\phi > \phi^{**}$. Thus,

$$\begin{aligned} G_{\text{dry}} &\approx \frac{k_{\text{B}}T}{N_{\text{el}} b^3} \phi_0^{2/3} \\ &\approx \frac{k_{\text{B}}T}{b^3} Q^{-4/(9\nu-3)} (\phi^{**})^{(6\nu-3)/(3\nu-1)} \end{aligned} \quad (\text{A27})$$

Comparing the expressions for modulus and order parameter in the dry state, we find that

$$\begin{aligned} G_{\text{dry}} &\approx \frac{k_{\text{B}}T}{N_{\text{el}} b^3} \phi_0^{2/3} \\ &\approx \frac{k_{\text{B}}T}{b^3} m_{\text{dry}} (\phi^{**})^{(2\nu-1)/(3\nu-1)} \end{aligned} \quad (\text{A28})$$

where the extra ϕ^{**} term displays exactly the above correction for extrapolating modulus up to $\phi = 1$.

Drying for Samples Prepared in the Good-Solvent Regime, $\phi_0 < \phi^{**}$. In the dry state, $\phi = 1$, eq A19 becomes

$$m_{\text{dry}} \approx \phi_0^{1/(9\nu-3)} (\phi^{**})^{(2\nu-1)/(3\nu-1)} N_{\text{el}}^{-1} \\ \approx Q^{-4/(9\nu-3)} (\phi^{**})^{(8\nu-4)/(3\nu-1)} \quad (\text{A29})$$

When extrapolating modulus at swelling equilibrium across ϕ^{**} up to ϕ , we recover eq A27 for the dry modulus as a function of Q in the intermediate case. Similarly, we expect the very same relation for the dry order parameter as a function of Q as before, eq A26. This leads again to

$$G_{\text{dry}} \approx \frac{k_{\text{B}}T}{b^3} m_{\text{dry}} (\phi^{**})^{(2\nu-1)/(3\nu-1)} \\ \approx \frac{k_{\text{B}}T}{b^3 N_{\text{el}}} \phi_0^{1/(9\nu-3)} (\phi^{**})^{(4\nu-2)/(3\nu-1)} \quad (\text{A30})$$

However, this relation depends in a different form on ϕ_0 and ϕ^{**} as compared to the intermediate case, see eq A28.

AUTHOR INFORMATION

Corresponding Author

Michael Lang – Leibniz Institut für Polymerforschung, 01069 Dresden, Germany; orcid.org/0000-0003-3851-6670; Email: lang@ipfdd.de

Authors

Reinhard Scholz – Leibniz Institut für Polymerforschung, 01069 Dresden, Germany

Lucas Löser – Martin-Luther Universität Halle-Wittenberg, Institute of Physics – NMR Group, D-06120 Halle/Saale, Germany; orcid.org/0000-0003-0141-7011

Carolin Bunk – Leibniz Institut für Polymerforschung, 01069 Dresden, Germany; Organic Chemistry of Polymers, Technische Universität Dresden, 01062 Dresden, Germany; orcid.org/0000-0002-9760-9255

Nora Friciczer – Johannes Gutenberg University Mainz, Department of Chemistry, D-55128 Mainz, Germany

Sebastian Seiffert – Johannes Gutenberg University Mainz, Department of Chemistry, D-55128 Mainz, Germany; orcid.org/0000-0002-5152-1207

Frank Böhme – Leibniz Institut für Polymerforschung, 01069 Dresden, Germany; orcid.org/0000-0001-6128-4658

Kay Saalwächter – Martin-Luther Universität Halle-Wittenberg, Institute of Physics – NMR Group, D-06120 Halle/Saale, Germany; orcid.org/0000-0002-6246-4770

Complete contact information is available at:

<https://pubs.acs.org/10.1021/acs.macromol.2c00589>

Notes

The authors declare no competing financial interest.

ACKNOWLEDGMENTS

The authors thank the Deutsche Forschungsgemeinschaft (DFG) for funding the research network FOR2811 under grant 397384169 and our work with grants 423478088, 423435302, 423373052, and 423435431. We also thank the ZIH Dresden for a generous grant of computing times.

REFERENCES

- (1) Guo, Y.; Bae, J.; Fang, Z.; Li, P.; Zhao, F.; Yu, G. Hydrogels and Hydrogel-Derived Materials for Energy and Water Sustainability. *Chem. Rev.* **2020**, *120*, 7642–7707.
- (2) Echeverria, C.; Fernandes, S. N.; Godinho, M. H.; Borges, J. P.; Soares, I. P. Functional Stimuli-Responsive Gels: Hydrogels and Microgels. *Gels* **2018**, *4*, 54.
- (3) Flory, P. J.; Rehner, J. Statistical Mechanics of Cross-Linked Polymer Networks II. Swelling. *J. Chem. Phys.* **1943**, *11*, 521–526.
- (4) Bray, J. C.; Merrill, E. W. Poly (vinyl alcohol) hydrogels. Formation by electron beam irradiation of aqueous solutions and subsequent crystallization. *J. Appl. Polym. Sci.* **1973**, *17*, 3779–3794.
- (5) Obukhov, S. P.; Rubinstein, M.; Colby, R. H. Network Modulus and Superelasticity. *Macromolecules* **1994**, *27*, 3191–3198.
- (6) Pütz, M.; Kremer, K.; Everaers, R. Self-Similar Chain Conformations in Polymer Gels. *Phys. Rev. Lett.* **2000**, *84*, 298–301.
- (7) Sommer, J.-U.; Lay, S. Topological Structure and Nonaffine Swelling of Bimodal Polymer Networks. *Macromolecules* **2002**, *35*, 9832–9843.
- (8) Panyukov, S.; Rubinstein, M. Explanation of Anomalous Scaling of Swollen Entangled Chains. *Macromolecules* **2005**, *38*, 3511–3514.
- (9) Lang, M.; Fischer, J.; Werner, M.; Sommer, J. U. Swelling of olympic gels. *Phys. Rev. Lett.* **2014**, *112*, 1–5.
- (10) Flory, P. J. Molecular Theory of Rubber Elasticity. *Polym. J.* **1985**, *17*, 1–12.
- (11) Rubinstein, M.; Panyukov, S. Nonaffine Deformation and Elasticity of Polymer Networks. *Macromolecules* **1997**, *30*, 8036–8044.
- (12) Chen, Z.; Cohen, C.; Escobedo, F. A. Monte Carlo Simulation of the Effect of Entanglements on the Swelling and Deformation Behavior of End-Linked Polymeric Networks. *Macromolecules* **2002**, *35*, 3296–3305.
- (13) Lang, M. Bildung und Struktur von polymeren Netzwerken, Dissertation. Ph.D. thesis, Universität Regensburg, 2004.
- (14) Svaneborg, C.; Grest, G.; Everaers, R. Strain-Dependent Localization, Microscopic Deformations, and Macroscopic Normal Tensionsin Model Polymer Networks. *Phys. Rev. Lett.* **2004**, *93*, 257801.
- (15) Lang, M. Monomer fluctuations and the distribution of residual bond orientations in polymer networks. *Macromolecules* **2013**, *46*, 9782–9797.
- (16) Lang, M. Relation between Cross-Link Fluctuations and Elasticity in Entangled Polymer Networks. *Macromolecules* **2017**, *50*, 2547–2555.
- (17) Gumbrell, S. M.; Mullins, L.; Rivlin, R. S. Departures of the elastic behaviour of rubbers in simple extension from the kinetic theory. *Trans. Faraday Soc.* **1953**, *49*, 1495–1505.
- (18) Klüppel, M. Finite Chain Extensibility and Topological Constraints in Swollen Networks. *Macromolecules* **1994**, *27*, 7179–7184.
- (19) Lang, M.; Göritz, D.; Kreitmeier, S. Intramolecular reactions in randomly end-linked polymer networks and linear (Co)-polymerizations. *Macromolecules* **2005**, *38*, 2515–2523.
- (20) Lange, F.; Schwenke, K.; Kurakazu, M.; Akagi, Y.; Chung, U.-I.; Lang, M.; Sommer, J.-U.; Sakai, T.; Saalwächter, K. Connectivity and structural defects in model hydrogels: A combined proton NMR and Monte Carlo simulation study. *Macromolecules* **2011**, *44*, 9666–9674.
- (21) Rebello, N. J.; Beech, H. K.; Olsen, B. D. Adding the Effect of Topological Defects to the Flory-Rehner and Bray-Merrill Swelling Theories. *ACS Macro Lett.* **2021**, *10*, 531–537.
- (22) Zhong, M.; Wang, R.; Kawamoto, K.; Olsen, B. D.; Johnson, J. A. Quantifying the impact of molecular defects on polymer network elasticity. *Science* **2016**, *353*, 1264–1268.
- (23) Lang, M. Elasticity of Phantom Model Networks with Cyclic Defects. *ACS Macro Lett.* **2018**, *7*, 536–539.
- (24) Lang, M. On the Elasticity of Polymer Model Networks Containing Finite Loops. *Macromolecules* **2019**, *52*, 6266–6273.
- (25) Sakai, T.; Matsunaga, T.; Yamamoto, Y.; Ito, C.; Yoshida, R.; Suzuki, S.; Sasaki, N.; Shibayama, M.; Chung, U.-I. Design and Fabrication of a High-Strength Hydrogel with Ideally Homogeneous

Network Structure from Tetrahedron-like Macromonomers. *Macromolecules* **2008**, *41*, 5379–5384.

(26) Lang, M.; Schwenke, K.; Sommer, J. U. Short cyclic structures in polymer model networks: A test of mean field approximation by monte carlo simulations. *Macromolecules* **2012**, *45*, 4886–4895.

(27) Schwenke, K.; Lang, M.; Sommer, J.-U. On the Structure of Star Polymer Networks. *Macromolecules* **2011**, *44*, 9464–9472.

(28) Sommer, J.-U.; Chassé, W.; Valentín, J. L.; Saalwächter, K. Effect of excluded volume on segmental orientation correlations in polymer chains. *Phys. Rev. E* **2008**, *78*, 051803.

(29) Jakisch, L.; Garaleh, M.; Schafer, M.; Mordvinkin, A.; Saalwächter, K.; Bohme, F. Synthesis and structural NMR characterization of novel PPG/PCL conetworks based upon hetero-complementary coupling reactions. *Macromol. Chem. Phys.* **2018**, *219*, 1700327.

(30) Bunk, C.; Löser, L.; Fricicz, N.; Komber, H.; Jakisch, L.; Scholz, R.; Saalwächter, K.; Seiffert, S.; Lang, M.; Voit, B.; Böhme, F. Synthesis of Amphiphilic Model Networks Based on PEG and PCL Four-Arm Star Polymers with Complementary Reactivity. *submitted*.

(31) Carmesin, I.; Kremer, K. The bond fluctuation method: a new effective algorithm for the dynamics of polymers in all spatial dimensions The Bond Fluctuation Method: A New Effective Algorithm for the Dynamics of Polymers in All Spatial Dimensions. *Macromolecules* **1988**, *21*, 2819–2823.

(32) Deutsch, H. P.; Binder, K. Interdiffusion and self-diffusion in polymer mixtures: A Monte Carlo study. *J. Chem. Phys.* **1991**, *94*, 2294–2304.

(33) Müller, T.; Wengenmayr, M.; Dockhorn, R.; Rabbel, H.; Knespel, M.; Checkervarty, A.; Sinapius, V.; Guo, H.; Werner, M. *LeMonADE-project/LeMonADE: LeMonADE v2.2.2*. **2021**, DOI: 10.5281/zenodo.5061542.

(34) Müller, T.; Wengenmayr, M.; Dockhorn, R.; Knespel, M. *LeMonADEproject/LeMonADE-GPU: Release v1.2*. **2021** DOI: 10.5281/zenodo.5513487.

(35) Romeis, D.; Lang, M. Excluded volume effects in polymer brushes at moderate chain stretching. *J. Chem. Phys.* **2014**, *141*, 104902.

(36) Klos, J.; Sommer, J.-U. Dendrimer solutions: a Monte Carlo study. *Soft Matter* **2016**, *12*, 9007–9013.

(37) Lang, M.; Schuster, C.; Dockhorn, R.; Wengenmayr, M.; Sommer, J.-U. Testing the physics of knots with a Feringa nanoengine. *Phys. Rev. E* **2018**, *98*, 052501.

(38) Müller, T.; Sommer, J.-U.; Lang, M. Tendomers - force sensitive bis-rotaxanes with jump-like deformation behavior. *Soft Matter* **2019**, *15*, 3671–3679.

(39) Michalke, W.; Lang, M.; Kreitmeier, S.; Göritz, D. Comparison of topological properties between end-linked and statistically cross-linked polymer networks. *J. Chem. Phys.* **2002**, *117*, 6300–6307.

(40) Lang, M.; Kreitmeier, S.; Göritz, D. Trapped Entanglements in Polymer Networks. *Rubber Chem. Technol.* **2007**, *80*, 873–894.

(41) Müller, T.; Sommer, J.-U.; Lang, M. Swelling of Tendomer Gels. *Macromolecules* **2021**, *54*, 4601–4614.

(42) Trautenberg, H. L.; Hölzl, T.; Göritz, D. Evidence for the Absence of Bond-Crossing in the Three-Dimensional Bond Fluctuation Model. *Comput. Theor. Polym. Sci.* **1996**, *6*, 135–141.

(43) Nedelcu, S.; Werner, M.; Lang, M.; Sommer, J.-U. GPU implementations of the bond fluctuation model. *J. Comput. Phys.* **2012**, *231*, 2811–2824.

(44) Paul, W.; Binder, K.; Heermann, D. W.; Kremer, K. Crossover scaling in semidilute polymer solutions: a Monte Carlo test. *Journal de Physique II* **1991**, *1*, 37–60.

(45) Wittmer, J. P.; Beckrich, P.; Meyer, H.; Cavallo, A.; Johner, A.; Baschnagel, J. Intramolecular long-range correlations in polymer melts: The segmental size distribution and its moments. *Phys. Rev. E* **2007**, *76*, 1–18.

(46) Lang, M.; Fischer, J.; Sommer, J. U. Effect of topology on the conformations of ring polymers. *Macromolecules* **2012**, *45*, 7642–7648.

(47) Kreer, T.; Baschnagel, J.; Müller, M.; Binder, K. Monte Carlo simulation of long chain polymer melts: Crossover from rouse to reptation dynamics. *Macromolecules* **2001**, *34*, 1105–1117.

(48) Lang, M.; Kumar, K. S. Simple and General Approach for Reversible Condensation Polymerization with Cyclization. *Macromolecules* **2021**, *54*, 7021–7035.

(49) Scanlan, J. The Effect of Network Flaws on the Elastic Properties of Vulcanizates. *J. Polym. Sci.* **1960**, *43*, 501–508.

(50) Case, J. Branching in Polymers. I. Network Defects. *J. Polym. Sci.* **1960**, *45*, 397–404.

(51) Lang, M.; Müller, T. On the modulus of non-entangled networks made of real chains. *submitted*.

(52) Baum, J.; Munowitz, M.; Garroway, A. N.; Pines, A. Multiple-quantum dynamics in solid state NMR. *J. Chem. Phys.* **1985**, *83*, 2015–2025.

(53) Wall, F.; Flory, P. J. Statistical Thermodynamics of Rubber Elasticity. *J. Chem. Phys.* **1951**, *19*, 1435–1439.

(54) Flory, P. J. *Principles of Polymer Chemistry*; Cornell University Press: Ithaca, NY, 1953; pp 1–672.

(55) James, H. M.; Guth, E. Theory of the Elastic Properties of Rubber. *J. Chem. Phys.* **1943**, *11*, 455–480.

(56) James, H. M. Statistical Properties of Networks of Flexible Chains. *J. Chem. Phys.* **1947**, *15*, 651–668.

(57) Ronca, G.; Allegra, G. An approach to rubber elasticity with internal constraints. *J. Chem. Phys.* **1975**, *63*, 4990–4997.

(58) Flory, P. J. Theory of elasticity of polymer networks. The effect of local constraints on junctions. *J. Chem. Phys.* **1977**, *66*, 5720–5729.

(59) Heinrich, G.; Straube, E. On the strength and deformation dependence of the tube-like topological constraints of polymer networks, melts and concentrated solutions. I. The polymer network case. *Acta Polym.* **1983**, *34*, 589–594.

(60) Heinrich, G.; Straube, E. On the strength and deformation dependence of the tube-like topological constraints of polymer networks, melts and concentrated solutions. II. Polymer melts and concentrated solutions. *Acta Polym.* **1984**, *35*, 115–119.

(61) Heinrich, G.; Kaliske, M. Theoretical and numerical formulation of a molecular based constitutive tube-model of rubber elasticity. *Comp. Theor. Polym. Sci.* **1997**, *7*, 227–241.

(62) Rubinstein, M.; Panyukov, S. Elasticity of polymer networks. *Macromolecules* **2002**, *35*, 6670–6686.

(63) Rubinstein, M.; Colby, R. H. *Polymer Physics*; Oxford University Press: Oxford, U.K., 2003.

(64) de Gennes, P.-G. *De Gennes - Scaling Concepts in Polymer Physics*; Cornell University Press: Ithaca/London, 1979.

(65) Clisby, N. Accurate Estimate of the Critical Exponent ν for Self-Avoiding Walks via a Fast Implementation of the Pivot Algorithm. *Phys. Rev. Lett.* **2010**, *104*, 055702.

(66) Adam, M.; Delsanti, M. Viscosity and longest relaxation time of semi-dilute polymer solutions. I. Good solvent. *J. Phys. (Paris)* **1983**, *44*, 1185–1193.

(67) Colby, R. H.; Fetters, L. J.; Funk, W. G.; Graessley, W. W. Effects of concentration and thermodynamic interaction on the viscoelastic properties of polymer solutions. *Macromolecules* **1991**, *24*, 3873–3882.

(68) De Gennes, P. G. Dynamics of Entangled Polymer Solutions. I. The Rouse Model. *Macromolecules* **1976**, *9*, 587–593.

(69) Pincus, P. Excluded Volume Effects and Stretched Polymer Chains. *Macromolecules* **1976**, *9*, 386–388.

(70) Cohen Addad, J. P.; Domard, M.; Herz, J. NMR observation of the swelling process of polydimethylsiloxane networks. Average orientational order of monomeric units. *J. Chem. Phys.* **1982**, *76*, 2744–2753.

(71) Sommer, J. U.; Saalwächter, K. Segmental order in end-linked polymer networks: A Monte Carlo study. *Eur. Phys. J. E* **2005**, *18*, 167–182.

(72) Lang, M.; John, A.; Sommer, J.-U. Model simulations on network formation and swelling as obtained from cross-linking co-polymerization reactions. *Polymer* **2016**, *82*, 138–155.

(73) Akagi, Y.; Matsunaga, T.; Shibayama, M.; Chung, U.-I.; Sakai, T. Evaluation of Topological Defects in Tetra-PEG Gels. *Macromolecules* **2010**, *43*, 488–493.

(74) Saalwächter, K. Proton multiple-quantum NMR for the study of chain dynamics and structural constraints in polymeric soft materials. *Prog. Nucl. Magn. Reson. Spectrosc.* **2007**, *51*, 1–35.

(75) Lang, M.; Sommer, J.-U. Analysis of Entanglement Length and Segmental Order Parameter in Polymer Networks. *Phys. Rev. Lett.* **2010**, *104*, 177801.

(76) Ball, R. C.; Callaghan, P. T.; Samulski, E. A simplified approach to the interpretation of nuclear spin correlations in entangled polymeric liquids. *J. Chem. Phys.* **1997**, *106*, 7352–7361.

(77) Chassé, W.; Schlögl, S.; Riess, G.; Saalwächter, K. Inhomogeneities and local chain stretching in partially swollen networks. *Soft Matter* **2013**, *9*, 6943–6954.

(78) Saalwächter, K.; Kleinschmidt, F.; Sommer, J.-U. Swelling Heterogeneities in End-Linked Model Networks: A Combined Proton Multiple-Quantum NMR and Computer Simulation Study. *Macromolecules* **2004**, *37*, 8556–8568.

(79) Chassé, W.; Lang, M.; Sommer, J.-U.; Saalwächter, K. Cross-Link Density Estimation of PDMS Networks with Precise Consideration of Networks Defects. *Macromolecules* **2012**, *45*, 899–912.

(80) Likos, C. N. Effective Interactions in Soft Condensed Matter Physics. *Phys. Rep.* **2001**, *348*, 267–439.

(81) Cohen Addad, J. P. Polymeric-gel swelling: NMR evidence for the c^* theorem. *Phys. Rev. B* **1993**, *48*, 1287–1290.

(82) Lang, M.; Göritz, D.; Kreitmeier, S. Length of subchains and chain ends in cross-linked polymer networks. *Macromolecules* **2003**, *36*, 4646–4658.

Recommended by ACS

Phantom-Chain Simulations for the Effect of Node Functionality on the Fracture of Star-Polymer Networks

Yuichi Masubuchi, Takashi Uneyama, *et al.*

SEPTEMBER 18, 2023

MACROMOLECULES

[READ !\[\]\(40867c266b2a72abe217a45bea6f736a_img.jpg\)](#)

Phase Separation and Gelation in Solutions and Blends of Heteroassociative Polymers

Scott P. O. Danielsen, Michael Rubinstein, *et al.*

JULY 10, 2023

MACROMOLECULES

[READ !\[\]\(9fb1b636af3d2fad1dccb5d437c240cb_img.jpg\)](#)

Foundation of Network Forensics

Andrey V. Dobrynin, Yuan Tian, *et al.*

NOVEMBER 15, 2023

MACROMOLECULES

[READ !\[\]\(ca8f242841660008ed3e2273f2a3d887_img.jpg\)](#)

Topologically Frustrated Dynamical State of Polymers Trapped in Ideal Uniform Tetra-PEG Gels

Di Jia, Murugappan Muthukumar, *et al.*

NOVEMBER 29, 2023

MACROMOLECULES

[READ !\[\]\(700de1146ce8d8d31c70e1dbe6152e98_img.jpg\)](#)

[Get More Suggestions >](#)